Structural control on shallow hydrogeochemical processes at Caviahue-Copahue Volcanic Complex (CCVC), Argentina

Daniele Tardani, Emilie Roulleau, Daniele L Pinti, Pamela Pérez-Flores, Linda Daniele, Martin Reich, Pablo Sanchez-Alfaro, Diego Morata, Luc Richard

Daniele Tardani, Emilie Roulleau, Daniele L Pinti, Pamela Pérez-Flores, Linda Daniele, et al.. Structural control on shallow hydrogeochemical processes at Caviahue-Copahue Volcanic Complex (CCVC), Argentina. Journal of Volcanology and Geothermal Research, 2021, 414, 10.1016/j.jvolgeores.2021.107228 . hal-03184971

HAL Id: hal-03184971
https://hal.univ-reunion.fr/hal-03184971

Submitted on 30 Mar 2021

Structural control on shallow hydrogeochemical processes at Caviahue-Copahue Volcanic Complex (CCVC), Argentina

Daniele TARDANI[1,2]*, Emilie ROULLEAU[3,4], Daniele L. PINTI[5,6,7], Pamela PERÉZ-FLÓRES[8], Linda DANIELE[2,9], Martin REICH[2,9], Pablo SÁNCHEZ[1,2], Diego MORATA[2,9], Luc RICHARD[5]

1 – Instituto de Ciencias de la Tierra, Universidad Austral de Chile, Valdivia, Chile

2 – Andean Geothermal Center of Excellence (CEGA), Universidad de Chile, Santiago, Chile

3 – Stratagem974, Sainte Clotilde, La Réunion, France

4 – Université de La Réunion, Laboratoire Géosciences Réunion, F-97744 Saint Denis, France

5 – GEOTOP and Département des Sciences de la Terre et de l'Atmosphère, Université du Québec à Montréal, Montréal QC, Canada

6 – Key Laboratory of Petroleum Resources, Gansu Province, Northwest Institute of Eco-Environment and Resources, Chinese Academy of Sciences, Lanzhou 730000, China

7 – Gansu Talent and Intelligence Center for Remediation of Closed and Old Deposits, Lanzhou 730000, China

8 – Consultoria e Investigación Geológico Ambiental Ltda. Huasco. Chile

9 – Department of Geology, Facultad de Ciencias Físicas y Matemáticas. Universidad de Chile, 8370450 Santiago, Chile

* Corresponding author: E-mail: daniele.tardani@uach.cl

Keywords: Helium isotopes; stable isotopes; radiocarbon; tritium; strontium isotopes; Copahue volcano.

Revised version to *Journal of Volcanology and Geothermal Research*

Abstract words: 319; Text words: 6921; References = 64; Figures = 8; Tables = 2

Abstract

The Caviahue-Copahue Volcanic Complex (CCVC) hosts one of Argentina's most important geothermal systems. To provide new insights into origin, circulation, and residence time of fluids, the chemical and isotopic composition ($^3He/^4He$, δ^2H-$\delta^{18}O$ in H_2O; $\delta^{13}C$-$\delta^{18}O$ in CO_2; $^{87}Sr/^{86}Sr$) of thermal waters was measured together with the ^3H and ^{14}C activities. Water samples were collected from hot springs (LM, TC, LMM, CB and AF) representing the five major thermal zones of the CCVC and assumed to be steam-heated meteoric waters, and a well condensate (COP-2). The LMM, CB, and AF chemical composition and $^{87}Sr/^{86}Sr$ ratios show that water chemistry is acquired locally from exchange with volcanic rocks (Sr, SiO_2, among others) and from steam (H_2S). Two surface geothermal manifestations (LM and TC), along with the well condensate, COP-2, contain a higher contribution of deep-originating fluids, with $^{87}Sr/^{86}Sr$ indicating possible contribution from deep-seated granitoids or sediments from the underlying basement. Radiocarbon-based residence times indicate ages ranging between 13,540 and 17,520 yrs BP, representing the minimum age for the geothermal reservoir waters. Tritium is mainly absent in hot spring waters except for LMM and CB where the activity is close to the detection limit. This indicates a minimum age older than 70 yrs for the water circulating in the shallow circuit. This result suggests that shallow meteoric water have a more complex and/or deeper circuit, resulting in older residence times. Helium isotopes in the CCVC span a wide range, from a pure mantle-derived value, of 8.35Ra, to a more crustal radiogenic signature, of 4.6Ra. The spatial variation is explained by associating the geochemical data with the geological context, which includes the distribution of fault-fracture meshes and different sources of magmatic volatiles underlying the Copahue volcano. The first order control on helium isotope signatures observed in this study seems to be dominated by the degree of crustal assimilation of the magmatic sources, which is in turn controlled by the local arrays of faults.

1. INTRODUCTION

The Copahue stratovolcano, part of the Caviahue-Copahue Volcanic Complex (CCVC), is an active volcano that hosts a high-enthalpy geothermal system (JICA, 1992) that represents a promising resource for geothermal energy in Argentina (Barcelona et al., 2020). The CCVC is located in the Southern Volcanic Zone (SVZ, 33 - 46 ° S) of the Andes, at the northern termination of the intra-arc, strike-slip, Liquiñe-Ofqui Fault System (LOFS). Here, a trans-tensional-NE transfer zone is developed, linking the LOFS and the Antiñir-Copahue Fault System (e.g. Sielfeld et al, 2017).

The geothermal area of interest lies to the north and northwest of the Copahue volcanic edifice, with several surface emissions including fumaroles, bubbling pools, mud pools and thermal springs, which are spatially associated with local extensional faults which act as fluid preferential pathways (Nakanishi et al., 1995; Melnick et al., 2006; Barcelona et al., 2019). The area has been studied extensively over the last thirty years, and, in the early 1990s, the Japanese International Cooperation Agency (JICA) carried out a deep drilling campaign and a feasibility study for developing a high-enthalpy geothermal field. Renewed interest in studying the processes controlling this hypothermal system was driven by the anomalous volcanic unrest of the Copahue volcano during the 2012-2016 period and by the possibility of developing potential geothermal resources in the Andean region (Barcelona et al., 2020). In recent years, several studies have focused on the geochemistry of the Copahue volcanic-hydrothermal system and its CO_2 surface degassing (Agusto et al., 2013; Agusto and Varekamp, 2016; Chiodini et al., 2015; Roulleau et al., 2016, 2017; Tassi et al., 2017; Lamberti et al., 2019). These studies have improved our understanding of the structural factors controlling the hydrothermal activity, and have provided crucial information to refine the conceptual model of the local fault-fracture hydraulic architecture in the Copahue geothermal system (Barcelona et al., 2019).

The goal of this study is to assess relevant processes acting in the hydrological system of Copahue, as the residence time of fluids, hydrothermal fluid sources and circulation patterns. In the present contribution are presented the first radiocarbon (^{14}C) activities together with strontium ($^{87}Sr/^{86}Sr$) isotope data measured in geothermal water samples collected from five thermal pools and a well steam condensate of the Copahue geothermal system. Together with new δ^2H, $\delta^{18}O$, $\delta^{13}C$-CO_2, $\delta^{18}O$-CO_2, ^3H, $^3He/^4He$, and $^4He/^{20}Ne$ data, they provide further insights into the residence times of deep and shallow fluids, the water–rock interaction processes, and the structural pathways that link the deep magmatic/geothermal system and the surface aquifers.

2. GEOLOGICAL SETTING OF THE CCVC GEOTHERMAL SYSTEM

The CCVC is located at 37.5°S and 71°W, at the border between Argentina and Chile in the Southern Volcanic Zone of the Andes and is composed of the Caviahue caldera and the Copahue stratovolcano (Fig. 1). The Caviahue caldera is a square-shaped depression of ca. 20 km × 15 km, defined as a trans-tensional pull-apart intra-arc basin due to the NE-transition zone between LOFS and the Copahue-Antiñir fault zone (Melnick et al., 2006).

The Copahue volcano is an active stratovolcano, situated on the western rim of the Caviahue caldera. Volcanic activity at Copahue began ca. 1 Ma ago. Since the Upper Pleistocene, volcanic activity has consisted mainly of andesitic lava flows and a few later-Holocene explosive episodes of andesitic to trachydacitic composition (Linares et al., 1999).

The Copahue geothermal system has developed at the northeastern part of the Copahue volcano, hosted in the Caviahue Caldera. The geothermal field mainly extends over the Copahue Village Fault System (Figure 1), composed of a set of extensional ~N˚60-striking faults – developed in a structural block between the Trolope and Chancho-có WNW-striking faults (Bonali et al., 2016;

Barcelona et al., 2019; 2020) – which affect the ignimbrites of the Las Mellizas volcanic sequence (JICA, 1992; Barcelona et al., 2020). Five active geothermal zones are recognized within the area, with evident surface manifestations consisting of hot springs, boiling pools, bubbling pools, and mud pools with temperatures of up to 96°C, and fumaroles that reach temperatures of up to 135°C (Agusto et al., 2013). The five thermal zones of Las Maquinas (LM), Las Maquinitas (LMM), Termas de Copahue (TC), Cabañita (CB), and Anfiteatro (AF) are located northeast of the volcano and appear to be spatially associated with NE- and WNW-striking fault systems (Melnick et al., 2006; Barcelona et al., 2019). The Chancho-có (CC) geothermal field is located on the northern flank of the volcano, in the WNW-striking Chancho-có Fault, in close proximity to the volcanic–hydrothermal system. The Pucon-Mahuida (PM) bubbling gas manifestation lies on the southern flank of Copahue volcano (Fig. 1). The complex fault systems interaction, under an extensional stress field, defines a NE-striking fault with high dilation tendency, while the WNW-striking faults are related to medium to low dilation tendency (Barcelona et al., 2019). This fault architecture controls the permeability and pathways of the hydrothermal fluids and meteoric water, and their isotopic and chemical variations (Barcelona et al, 2019).

The geothermal system at depth is characterized by a layered reservoir containing a shallow steam cap at 1000 m depth and a liquid-dominated level below 2000 m depth (Barcelona et al., 2019). The reservoir is located within Pliocene volcanic and volcaniclastic rocks, with a temperature higher than 270°C (JICA, 1992; Agusto et al., 2013; Barcelona et al., 2019; 2020). The reservoir has pervasive propylitic alteration. The upper thermal boundary includes a clay cap, which correlates with the andesitic deposits of the Las Mellizas Formation, affected by an advanced argillic alteration (Mas et al., 1995; Barcelona et al., 2019; 2020).

The surface geothermal pools in the geothermal/fumarolic areas around the volcano edifice are assumed to be steam-heated meteoric waters, partially evaporated as those in the crater lake, as indicated by the water stable isotope composition (e.g., Agusto et al., 2013; Agusto and Varekamp, 2016). The stable isotopic composition of the local meteoric water endmember is assumed to be $\delta^{2}H$ = -80±5 ‰ and $\delta^{18}O$ = -11.2±0.4‰ vs SMOW (Panarello, 2002) which is somehow in between the theoretical values for precipitations calculated using the Online Isotope Precipitation Calculator (OIPC; Bowen, 2017) at the 2965 m Copahue summit ($\delta^{2}H$ = -90 ‰, $\delta^{18}O$ = −12.6 ‰) and at the base of the edifice at the town of Caviahue ($\delta^{2}H$ = -70 ‰, $\delta^{18}O$ = −9.9 ‰) (Agusto and Varekamp, 2016). The hydrological model developed by Agusto et al. (2013) suggests that the volcanic-hydrothermal system underlying Copahue active crater consists of glacial meltwater that is acidified by magmatic gases uprising the magmatic chamber.

The weather in the region is typical of Andes, with precipitations over 2.000 mm/yr, mainly snow, covering about 200 days/yr (from April to October). The temperatures are about 25˚C on summer and -14˚C on winter, with an annual average of 7˚C (Mas et al., 2000). There are not isotopic data on precipitations at Copahue, either stable isotopes of water or tritium, as those collected by the Global Network of Isotopes in Precipitation (GNIP) of the International Atomic Energy Agency, in order to compare with values measured in water in this work or previous ones. Tritium data are scarce and mainly from stations located close to Buenos Aires except for a few data (n= 4) from the station of Cerro Ancasti at 1800m of altitude in the Andes, but 1016 km north of Copahue. The tritium activity is 12.3±1.6 Tritium units (TU) which is within the average for all Argentina (n = 87) of 11.1±3.3 TU (WISER database at http://www-naweb.iaea.org/napc/ih/IHS_resources_isohis.html).

3. METHODS

3.1 Sampling procedures

Figure 1 shows locations of sampled hot springs and their association with the main surface structural features of the Copahue geothermal area. Five hot spring water samples were collected from the five thermal zones recognized at Copahue (AF, CB, LM, LMM, TC; Fig. 1). Four geothermal exploration wells were drilled in the area (COP-1 to COP-4; Mas, 2005), but only one (COP-2) is currently accessible for sampling and both the liquid phase (as steam condensate) and the gas phase were collected.

Temperature, electric conductivity, and pH were measured *in situ*, and ionic balance computation was carried out, based on the method described by Giggenbach and Gouguel (1989). Water samples were filtered using a 0.45 μm filter (cellulose acetate) into precleaned, high density polythene bottles (250 ml for cations, anions, and Sr isotopes; 500 ml for ^3H and ^{14}C) being careful to avoid degassing or atmospheric CO_2 contamination for ^{14}C analyses. Samples for cations and trace element analyses were acidified with HNO_3 (Merck Suprapur®) 4N, 1 ml per 100 ml sample. Samples for silica content determination were diluted at a ratio of 1:10 with milliQ water in order to avoid silica precipitation. Water samples for stable isotopes of water were poured into 30 mL HDPE bottles, filled to the top, and closed avoiding the trapping of air bubbles. Water and bubbling gas for helium isotopes and for C and O isotopic analyses of CO_2 were collected in refrigeration-type copper tubes sealed with clamps at both extremities, using armed PVC tubes connected to a plastic funnel.

3.2 Analytical methods

Analyses of major anions and cations, and trace elements were performed at the Fluid Geochemistry Laboratory of the Andean Geothermal Center of Excellence (CEGA), at University of Chile, Santiago. Anion (F, Cl, and SO_4) concentrations were measured by ion chromatography (Dionex™ ICS-2100), while HCO_3 and CO_3 concentrations were determined by volumetric titration. Cations concentrations (Na, K, Ca, Mg) were determined by atomic absorption spectrometry (Perkin Elmer, PinAACle^{TM} 900F). Trace elements concentrations were determined by inductively coupled plasma mass spectrometry (Thermo Scientific, iCAP Q ICP-MS). Silica contents were measured with spectrophotometry (Hanna Instruments HI 96705).

Stable isotopes of water (δ^2H and δ^{18}O) and CO_2 (δ^{13}C and δ^{18}O), strontium isotopic ratios (^{87}Sr/^{86}Sr), and helium isotopic ratios (^{3}He/^{4}He) were determined at GEOTOP, University of Quebec in Montreal.

A 0.2 ml volume of sample water was pipetted into a 3 ml vial, closed with a septum cap, and transferred to a 40˚C heated rack. For δ^2H, a hydrophobic platinum catalyst (Hokko beads) was added. After one hour, air in the vials was replaced with CO_2 (for δ^{18}O) or H_2 (for δ^2H) using the AquaPrep. Samples were left to equilibrate for 7 hours for δ^{18}O and 4 hours for δ^2H. The equilibrated samples were analyzed with a Micromass model Isoprime isotope ratio mass spectrometer coupled to an AquaPrep system in dual inlet mode at the *Light stable isotope geochemistry laboratory* of the GEOTOP. Three internal reference waters were used to normalize the results on the V-SMOW-SLAP scale. A fourth reference water was analyzed as an unknown to assess the normalization. Results are given in delta units (δ) in ‰ vs VSMOW. The overall analytical uncertainty (1σ) is better than ±0.1‰ for δ^{18}O and ±2.0 ‰ for δ^2H.

The CO_2 was separated from residual humidity in the copper tube, if any, using an isopropyl dry ice mix trap, and a liquid nitrogen trap was used to separate CO_2 from other incondensable gases, following procedures described in Richard et al. (2019). Because the amount of residual water is negligible, even at ambient temperature the exchange of ^{18}O between water and CO_2 will not affect the δ^{18}O-CO_2 (Richard et al., 2019). Indeed Figure 3 shows that CO_2-H_2O re-equilibration occur *in situ* at geothermal pool temperatures of 90-100˚C. After recovering a variable amount of CO_2 gas in a Pyrex glass vessel, the isotopic compositions of C and O were determined using an Isoprime 100 Dual Inlet Isotope Ratio Mass Spectrometer (DI-IRMS) at the *Light stable isotope geochemistry laboratory* of the GEOTOP (Richard et al., 2019). The samples were compared to a working CO_2 standard that had been normalized to the V-PDB scale.

Strontium isotopic ratios ($^{87}Sr/^{86}Sr$) were analyzed in water samples and the liquid condensate of COP-2 well by thermal ionization mass spectrometry (TIMS Triton plus) at the *Radiogenic and non-traditional stable isotope geochemistry laboratory* of GEOTOP. This technique requires the chemical separation of Sr, which was carried out by evaporating the water sample on a hot plate, and then uptaking the salt in 3 mol/L HNO_3. The obtained solution was centrifuged and purified onto a Sr-spec ion exchange column to extract the Sr in HNO_3 3N/0.05N high purity reagents. The solution is then pipetted on a filament to be analyzed by TIMS. The NBS987 standard (100ng) was measured at 0.71026±0.00002 at the beginning of the analytical session, obviously on a separate filament and thus eliminating any “memory” effect on samples.

The isotopic ratios of He ($^3He/^4He$) were measured using a noble gas mass spectrometer at the *Montreal Noble Gas Laboratory (GRAM)* of GEOTOP. The gas mixture in the copper tubes was diluted manually in a specific volume until pressure, measured on a Baratron Gauge, was less than 10 mbar. The reactive gases were removed using one Ti-getter at 600 °C for 15 min followed by 10 min at ambient temperature and two SAES ST-707 getters at 100 °C for 15 min followed by 10 min at ambient temperature. Gases were then adsorbed onto an Advanced Research System (ARS®) cryogenic trap containing activated charcoal at 10K and released sequentially at 35K (He) and 110K (Ne). He and Ne isotopes were measured on a Thermo® HELIX-MC using the axial Faraday detector by peak jumping, except for ^3He, which was measured by ion counting on the axial Compact Discrete Dynode™ (CDD) detector. Blanks are typically on the order of 0.01% for He and Ne. Obtained signals were calibrated against a known aliquot of standard air. Typical standard reproducibility for ^{4}He and ^{20}Ne are 1.5–2%. Errors on the ^{3}He/^{4}He ratios are about 2% at 1σ.

Assuming that the Air Saturated Water (ASW) neon content is significantly higher than in mantle and crustal gases, the measured ^{3}He/^{4}He ratio, normalized to that of the atmosphere Ra = 1.384 x 10^{-6} or R/Ra can be corrected for the presence of atmospheric helium (Rc/Ra) using the ^{4}He/^{20}Ne ratio of the sample (Craig et al., 1978):

$$R_c/R_a = [R/R_a - r]/(1-r), \qquad (1)$$

where “r” is defined as:

$$r = \left({}^{4}He/{}^{20}Ne \right)_{ATM} / \left({}^{4}He/{}^{20}Ne \right)_{obs}, \qquad (2)$$

where (^{4}He/^{20}Ne)$_{ATM}$ and (^{4}He/^{20}Ne)$_{obs}$ are the atmospheric and measured ^{4}He/^{20}Ne ratios respectively. If air is accidentally added during sampling the (^{4}He/^{20}Ne)$_{ATM}$ is equal to that of the atmosphere ((^{4}He/^{20}Ne)$_{Air}$ = 0.3185), while if it assumed that atmospheric He and Ne derive from the meteoric water endmember it should be calculated at the ASW conditions of temperature (MAAT or Mean Annual Average Temperature) which in Copahue is 11˚C ((^{4}He/^{20}Ne)$_{ASW}$ = 0.274; solubility data of Smith and Kennedy, 1983). For sake of consistency with previous results from the same area (e.g., Agusto et al., 2013; Tassi et al., 2017), the (^{4}He/^{20}Ne)$_{Air}$ = 0.3185 was retained as value for air correction.

Radiocarbon (^{14}C) was determined for the dissolved inorganic carbon (DIC) fraction on a 3MV accelerator mass spectrometer (AMS) at the University of Ottawa. The ^{12,13,14}C^{+3} ions were measured at 2.5 MV terminal voltage with Ar stripping (Crann et al., 2017). Radiocarbon contents are reported as modern carbon fraction (F^{14}C), according to Reimer et al. (2004), calculated using the ^{14}C/^{12}C ratios of the sample and the oxalic acid standard. All values were corrected and normalized using the $\delta^{13}C$ ratios and the same standard; the calculations are shown in Reimer et al. (2004). Calibration was performed using OxCal 4.2.4 software. Finally, the ages were calculated using the formula (Stuiver and Polach, 1977):

$$^{14}C \text{ years BP} = -8033 \ln (F^{14}C) \qquad (3),$$

where BP stands for "Before Present" and corresponds to the year 1950.

Tritium concentrations were analyzed at the Environmental Isotope Laboratory (EIL) at the University of Waterloo, Canada. Liquid Scintillation Counting (LSC) was used for tritium analyses. The samples were concentrated 15 times by electrolysis prior to performing the count. The detection limit for the enriched samples is 0.8 TU (Heemskerk and Johnson, 1998).

4. RESULTS AND DISCUSSION

Table 1 reports the concentrations of major ions and trace elements measured in the water samples from the five hot springs, and one steam condensate from the geothermal well. Table 2 reports the stable isotopic composition of water, CO_2, the $^{87}Sr/^{86}Sr$ ratios, the $^{3}He/^{4}He$ ratio (R/Ra), the $^{4}He/^{20}Ne$ ratio, and the air-corrected Rc/Ra. Finally, the ^{14}C activity (as a fraction of present-day activity or 120 pMc) and that of ^{3}H (TU) are also reported in Table 2.

4.1 Water chemical composition

The temperatures of sampled waters ranged from 55.4 °C to 93.5 °C. Well COP-2 presented a vapor temperature of 220°C. The condensate from COP-2 should have a temperature of 92°C, corresponding to the water boiling point at the well-head elevation of approximately 2075 m.a.s.l. Hot spring samples LMM, LM, AF, and CB show highly acidic pH (1.9 to 2.4), and their chemical compositions are dominated by SO_4 (496 to 6515 mg/L) as the principal anion, classifying them as steam-heated acid-sulfate waters (Giggenbach and Stewart, 1982). Hot spring sample TC shows a neutral pH of 6.8, with HCO_3 as the dominant chemical species. The HCO_3 in geothermal waters could be produced by the reaction of CO_2 with Na-K silicates, by the dissolution of carbonates, or by the direct dissolution of CO_2 in water, especially where there are high fluxes of this gas (Fournier and Truesdell, 1970; Gizaw, 1996). Previous studies carried out in the Copahue area showed significant CO_2 fluxes (average value of 112.25 g $m^{-2}d^{-1}$; Roulleau et al., 2017) from soil gases, which are related to local tectonic structures (Chiodini et al. 2015; Roulleau et al., 2017; Lamberti et al., 2019). The chemical composition of sample TC may be derived from the interaction of surface waters with a high-CO_2 concentration steam, relative to acid gas species, such as H_2S, HCl and HF.

Sample COP-2 corresponds to the condensed steam from COP-2 well, which reaches the vapor-dominated geothermal reservoir at 1400 m b.g.l (Sierra et al., 1992; Panarello, 2002). The alkaline pH (8.5) and the predominance of dissolved HCO_3 (33.3 mg/L) likely corresponds to CO_2 dissolution, while the much lower concentrations of Cl (0.9 mg/L) and SO_4 (0.81 mg/L) are likely due to the dissolution of HCl and H_2S. Therefore, these results show that CO_2 is the dominant gas in the dry steam phase at depth, in accordance with the gas composition, which shows a CO_2 concentration of 870 to 989 mmol/mol, significantly higher than the concentration of H_2S (2.5 - 150 mmol/mol) (Agusto et al., 2013; Roulleau et al., 2016).

Trace elements present a wide range of concentrations, varying from a few μg/L to hundreds of mg/L. Iron and Al are the most abundant elements, presenting concentrations ranging from 27.9 μg/L to 253 mg/L and 26.8 μg/L to 756 mg/L respectively. Manganese and B present concentrations varying from 10.5 μg/L to 3.5 mg/L and 1.4 μg/L to 5.5 mg/L respectively. Concentrations of Li, Rb, Sr, Ba, Cs, As, Cr, and Ni are in lower, ranging from fractions to hundreds of μg/L (Table 1).

Figure 2a-f shows trace elements plotted versus the SO_4 contents measured in the hot spring samples and the well condensate. The positive correspondence between SO_4 and Al, Fe, Mn, Rb, As, and Cs supports the hypothesis of a progressive isochemical dissolution of the host rocks due to the acidic and immature nature of the waters (Stefánsson and Arnórsson, 2005). Silica contents of the hot spring samples vary from 54.25 (LM) to 369 (LMM) mg/L, and, consistent with the trace element data, the highest concentrations are related to samples CB, LMM, and AF, suggesting that the SiO_2 origin is dominated by rock dissolution at the surface.

4.2. Stable isotope composition of sampled waters and gas phases

The $\delta^{13}C\text{-}CO_2$ values for the hot spring samples and COP-2 (Table 2) range between -7.81 ‰ and -7.23 ‰ versus V-PDB, typical of magmatic CO_2 (-6±2‰; Javoy et al., 1986) and similar to values measured by Agusto et al. (2013) in the same areas. $\delta^{18}O\text{-}CO_2$ ranges between -3.31 and +5.45‰ versus V-PDB. In hydrothermal system, variations in $\delta^{18}O\text{-}CO_2$ are expected to be controlled by the ^{18}O exchange between steam and CO_2 (Chiodini et al., 2000), the extent of which depends on the temperature at which this exchange proceeds and the initial ^{18}O composition of H_2O and CO_2. In Figure 3, the fractionation factor "α" between CO_2 and H_2O of ^{18}O is reported versus the inverse of the measured temperature at the hot spring or in the well. The isotopic equilibrium between H_2O and CO_2 is represented by the "per mil fractionation" or "1000lnα", which is calculated as follows (Chiodini et al., 2000):

$$1000 \ln \alpha_{CO2\text{-}H2O} = [(1000 + \delta^{18}O_{CO2}) / [(1000 + \delta^{18}O_{CO2})] \qquad (4)$$

The three curves reported in Fig. 3 represent the variation in 1000 ln $\alpha_{CO2\text{-}H2O}$ with temperature, as calculated by Friedman and O'Neil (1977), Richet et al. (1977), and the experimental curve of Chiodini et al. (2000). The sampled waters show $\delta^{18}O\text{-}CO_2$ in equilibrium with the ^{18}O of water, except for the condensate, COP-2, which shows a higher 1000 ln $\alpha_{CO2\text{-}H2O}$ value, perhaps indicative of incomplete re-equilibration, as observed in other geothermal wells in Larderello (Panichi et al., 1977) and in Mexico (Richard et al., 2019).

The results showed in Fig. 3 indicate that a re-equilibration took place between the CO_2 and the H_2O in our samples and thus the oxygen isotopic composition of water needs to be corrected of such a re-equilibration. The $\delta^{18}O$ of H_2O corrected for the exchange with the CO_2 or $\delta^{18}O^{f}_{H2O}$ can be calculated following the equation (Karolyté et al., 2017):

$$\delta^{18}O^{f}_{H2O} = \left(\delta^{18}O^{i}_{CO2} - 1000\ln\alpha\right) \times X_{CO2} + \delta^{18}O^{i}_{H2O} \times \left(1 - X_{CO2}\right) \quad (5),$$

where X_{CO2} is the fraction of oxygen in the system sourced from the CO_2. Based on steam/gas ratios and CO_2 molar contents in the geothermal surface pools sampled by Agusto et al. (2013), the X_{CO2} was estimated to vary between 0.026 to 0.037. Correction is practically nil for samples LM, AF and COP-2, while the isotopic shift in the $\delta^{18}O^{f}_{H2O}$ range from 0.11‰ for sample Tc and 0.55‰ for samples CB and LMM (Table 2).

Figure 4 shows the δ^2H versus $\delta^{18}O$ diagram of the sampled waters and the condensate of COP2 well, together with the local meteoric water line (LMWL), as calculated by local rainfall data from Agusto and Varekamp (2016). The term "EVAP" refers to the evaporation line which shows the effects of evaporation of pure meteoric waters at mean ambient temperatures (about 11 °C) and local relative humidity (60 %). This was calculated by Agusto and Varekamp (2016) to explain the stable isotopic composition of evaporated surface waters from streams, some geothermal pools and the crater lake.

The measured δ^2H and the CO_2-corrected $\delta^{18}O$ correlates and the calculated straight line passes through the meteoric water endmember defined by Panarello (2002) of δ^2H of -80‰ and a $\delta^{18}O$ -11‰ and an andesitic water source, as defined by Taran and Zelenski (2015). The straight line has a lower slope than the evaporation line, and equal to $\delta^2H = 3.2 \times \delta^{18}O - 45.2$, which is compatible, within the 95% confidence interval, with that calculated by Agusto and Varekamp (2016), of $\delta^2H = 3.6 \times \delta^{18}O - 41.65$ for the fluids that define the local Copahue volcano-hydrothermal system. The $\delta^{18}O$ does not show any pronounced horizontal shift toward higher values, which could indicate little water-rock interaction processes within the hydrothermal system, as suggested by Agusto et al. (2013).

4.3 $^{87}Sr/^{86}Sr$ isotope ratios: sources and water/rock interaction effects

Strontium isotopic ratios ($^{87}Sr/^{86}Sr$) of sampled hot springs and well condensate COP-2 are listed in Table 2. The measured $^{87}Sr/^{86}Sr$ ratios cover a narrow range between 0.70396±0.00006 (AF) to 0.70452±0.00013 (LM) with except the COP-2 condensate which shows a more radiogenic value of 0.70697±0.00039 (Table 2). The distribution of strontium between water and rocks is mainly determined by dissolution or by equilibrium isotope exchange between the rock and the fluid and $^{87}Sr/^{86}Sr$ generally reflect those of the host rock (Notsu et al., 1991).

In Figure 5, $^{87}Sr/^{86}Sr$ ratios are plotted against the temperature of the sampled geothermal water (a), the SiO_2 contents (b) and the $\delta^{13}C-CO_2$ (c). The orange area in Figs. 5a-c delineates the range of strontium isotopic signatures of the rock units composing the CCVC. These are trachyandesites to rhyolites from the Riscos Bayos ignimbrite, the 2000 eruption of Copahue and the caldera wallrock from Caviahue measured by Varekamp et al. (2006) (^{87}Sr/^{86}Sr from 0.70376±0.00002 to 0.70399±0.00002); volcanic sequences of the Cola de Zorro (Hualcupen) Fm. with a ^{87}Sr/^{86}Sr ratio of 0.70393±0.00003 (Roulleau et al., 2018); the ignimbrites of Las Mellizas (^{87}Sr/^{86}Sr = 0.70387±0.00003; Roulleau et al., 2018); and the Copahue volcanic series (^{87}Sr/^{86}Sr = 0.70389±0.00007 to 0.70405±0.00002; Roulleau et al., 2018), including recent lavas erupted by the Copahue volcano. These ^{87}Sr/^{86}Sr values are higher than those expected for a back-arc basaltic source (0.70330; Varekamp et al., 2006) and it has been explained by local contamination of the magma source with material from the subducting Nazca plate sediments (Pacific Ocean detrital sediments in Varekamp et al., 2006).

The ^{87}Sr/^{86}Sr values reported for LMM, CB, and AF are within the range of values measured in the volcanic rocks composing the CCVC (Figs. 5a-c) whereas samples TC, LM, and COP-2 present higher ^{87}Sr/^{86}Sr values, suggesting mixing with a fluid with higher radiogenic ^{87}Sr/^{86}Sr and which could be the endmember composition measured in COP-2. Sample COP-2 shows the highest radiogenic ^{87}Sr/^{86}Sr ratio of 0.70697, but the lowest SiO$_2$ concentration (Fig. 5b), which could appear strange at first sight. However, COP-2 represents the steam condensate from the steam cap lying above the geothermal reservoir, at a depth of ~1000 m (Barcelona et al., 2019), resulting from the boiling of reservoir water at depth. Thus, it is normal that SiO$_2$ has partitioned mostly in the liquid phase at depth and that the condensate is deprived of silica, but still conserves the original ^{87}Sr/^{86}Sr ratio.

The ^{87}Sr/^{86}Sr ratio measured in COP-2 condensate is anomalously high compared the other measured values (Table 2). High ^{87}Sr/^{86}Sr ratios are not found in volcanic rocks of this area but are common for the northern Southern volcanic zone (Varekamp et al., 2006), which is strongly affected by contributions from the subducting Nazca plate sediments. The radiogenic ^{87}Sr/^{86}Sr value measured in COP-2 has likely a local source and could be inherited either 1) from depth-seated granitoids or 2) from the Neuquén marine sequence, located 2 km below sea level under the Copahue-Caviahue volcanic sequence (Varekamp et al., 2006). At depths of 1000 m below ground level, at the bottom of the drill cores, the presence of a porphyritic intrusive body has been recognized (JICA, 1992). The fluid-rock interaction with such an intrusive unit may have shifted the $^{87}Sr/^{86}Sr$ ratios of fluids toward more radiogenic signatures than those characteristics of fluids having interacted with the Plio-Quaternary volcanic sequences of the CCVC. Porphyry generally show high $^{87}Sr/^{86}Sr$ ratios, with values of up to 0.7050-0.7080 (e.g., Thorpe et al., 1981; Maydagan et al., 2016). Varekamp et al. (2006) suggested the contribution of local sediments from the Nequém basin marine sequence to explain, i.e. the $\delta^{13}C$-CO_2 measured in the geothermal gases which are up to -8‰ vs V-PDB. Though the $\delta^{13}C$-CO_2 value is within the range expected for mantle carbon ($\delta^{13}C$ = - 6±2‰; Javoy et al., 1986) particularly in volcanic arcs (Mason et al., 2017), Varekamp et al. (2006) suggested that isotopically lighter carbon from organic-rich sediments could have contributed to the CO_2 of the CCVC gaseous manifestations. It is interesting to note in Fig. 5c, that the $^{87}Sr/^{86}Sr$ ratio vs the $\delta^{13}C$-CO_2 suggests a mixing between two fluids with different C and Sr isotopic composition (the mixing should be a hyperbola as represented in Fig. 5c). The fluid represented by the condensate of COP-2 is more enriched in radiogenic Sr and in isotopically lighter C, suggesting possible crustal Sr and C addition to the mixture.

4.4 $^3He/^4He$ isotope ratios: meteoric, crustal and mantle contributions

The helium isotopic ratio (R/Ra) of the hot springs and well COP-2 vary between 4.6Ra (AF) and 8.28Ra (LMM) (Table 2; Fig. 6), and values are consistent with those measured in previous studies (Agusto et al., 2013; Roulleau et al., 2016; 2018; Tassi et al., 2017). Overall, R/Ra values of the Copahue fluids are significantly higher than the atmospheric value (R/Ra = 1.0) and the crustal value (R/Ra = ~0.02Ra; Morrison and Pine, 1955), indicating a dominant mantle He contribution (R/Ra=8.0 ± 1; Allègre et al., 1995; Fig. 6), diluted locally by the addition of radiogenic and/or atmospheric ^{4}He.

The mixing hyperbolas plotted in Fig. 6 suggest that the He isotopic composition of LM, LMM, CB, and TC waters results from mixing between 1) deep-seated fluids containing mantle He with R/Ra values between 7 Ra and 9 Ra and either 2) air (R/Ra = 1 and ^{4}He/^{20}Ne = 0.3185) or 3) meteoric water containing dissolved atmospheric He at ASW conditions. In the case of Copahue geothermal field, recharge has been identified to be in Chancho-có and Anfiteatro areas, in addition to the water recharge occurring on the flank of the Copahue volcano (Agusto et al., 2013). The Mean Annual Air Temperature (MAAT) in this area is 11˚C (Agusto and Varekamp, 2016) leading to a ^{4}He/^{20}Ne ratio in the meteoric water at the recharge of 0.274 (using solubility data from Smith and Kennedy, 1983).

Samples COP-2 and AF pass through a hyperbola curve that suggests mixing between either air or meteoric water and geothermal waters having accumulated some radiogenic ^{4}He, with resulting lower R/Ra values of the second endmember of 6.5 and 4.0, respectively. The contribution of radiogenic (crustal) helium to the mixture can be determined using ternary mixing equations (Pinti et al., 2019):

$$R/Ra_{obs} = R/Ra_{mtl}*M+R/Ra_{crust}*C+R/Ra_{ASW}*A \qquad (6)$$

$$1/(^4He/^{20}Ne)_{obs} = M/(^4He/^{20}Ne)_{mtl}+ C/(^4He/^{20}Ne)_{crust}+ A/(^4He/^{20}Ne)_{ASW} \qquad (7)$$

$$M+C+A = 1 \qquad (8),$$

where the subscripts obs, mtl, crust, and ASW refer to the observed sample, the mantle end-member, the crustal end-member, and the freshwater end-member respectively and M, C, and A are the proportions of the three above-listed components. The radiogenic helium fraction is 19.6% of the total helium in the COP-2 condensate, and up to 42.1% in sample AF. The other parameter that seems to be related to water-rock interaction, namely the $^{87}Sr/^{86}Sr$ ratio, does not show a clear relationship with the helium isotopic composition of water, particularly for these two samples (COP-2 and AF). This could be due to different fluid ascent pathways through the field, with COP-2 and AF exchanging radiogenic ^{87}Sr with different reservoir and/or basement rocks.

4.5 ^{3}H and ^{14}C data: water residence time

The activities of both ^{3}H and ^{14}C were measured in well condensate COP-2 and in the hot springs LM, LMM, CB, TC, and AF (Table 2). The ^{14}C should provide a direct measure of water residence times in the range of 1 to 40 ka, whereas the abundance of ^{3}H reflects recharge processes since the atomic bomb test period in the 1950s and early 1960s (Birkle et al., 2001; Aggarwal, 2013). Unfortunately, there have been few attempts to use these two water chronometers in geothermal systems (e.g., Le Goff and McMurtry, 2000; Birkle et al., 2016; Morata et al., 2019) because geothermal waters often have residence times beyond the limit of the ^{3}H method (Goff & Janik, 2000), and only shallow hydrothermal circuits can be dated using this method, such as, for example, Beppu in Japan (Kitaoka, 1990) and Poás Volcano in Costa Rica (Rowe et al., 1995). Furthermore, the dominant volatile species in geothermal reservoirs is often volcanic CO_2, which constitutes an infinite pool of dead carbon masking the cosmogenic ^{14}C activity (e.g., Birkle et al., 2016).

The ^{14}C activity was measured in three of the six samples, with very little activity fraction values, of 0.113±0.0013 (LM), 0.1651±0.0014 (COP-2), and 0.1853±0.0018 (TC) (Table 2). The

^{14}C calculated ages yield values of 13,540±80 yrs BP for sample TC, 14,470±69 yrs BP for sample COP-2, and 17,520±93 yrs BP for sample LM (Table 2). Samples LMM, AF, and CB, where radiocarbon was not detected, presented a dissolved organic carbon (DOC) content 10 to 25 times higher than the DIC (Table 2).

Very low tritium activity of 0.8 TU, close to the detection limit of the method, was determined only in two samples, LMM and CB (Table 2). This suggests that waters have residence times older than 70 yrs, although a precise age cannot be estimated. This result is important because the general interpretation on the origin of the geothermal pools on the Copahue volcano flanks is steam-heated glacial meltwater infiltrating the summit crater (at ~3000 m.a.s.l.) and emerging at lower altitudes of 1600 m.a.s.l. It would expect that these waters have very short residence times, while both ^{3}H and ^{14}C data suggest the contrary. This could imply either 1) that the infiltrating meteoric water flow through a more complex and deeper hydrogeological circuit or 2) that they are mixed with an older water component.

Figure 7a shows the δ^{2}H of water versus the ^{4}He/^{20}Ne ratio. This latter ratio can indicate the degree of air contamination of a noble gas water sample or represent the ratio of atmospheric ^{4}He and ^{20}Ne dissolved in the meteoric water at the recharge (ASW conditions). Except for samples CB and LMM, the ^{4}He/^{20}Ne ratio correlated with the δ^{2}H value of water. This supports the hypothesis that ^{4}He/^{20}Ne variability indicates the mixing between meteoric water showing ASW-like ^{4}He/^{20}Ne ratios, and geothermal water, showing a heavier, "andesitic", δ^{2}H composition and a higher ^{4}He/^{20}Ne ratio due to addition of terrigenic ^{4}He. This result does not agree with the general interpretation of the Copahue geothermal pools being steam-heated meteoric waters. If it is the case, we should not see any correlation between ^{4}He/^{20}Ne – transported by the steam phase –and the stable isotopic composition of the hydrogen in the water phase. This can be the case of samples

CB and LMM which indeed do not follow this general trend. From the δ^2H values of the two possible endmembers (δ^2H = -80‰ for meteoric water; Agusto and Varekamp, 2016; δ^2H = -20‰ for the andesitic water; Giggenbach, 1992) and using a simple binary mixing equation, the fraction of "andesitic water" in sample AF is practically nil but increase up to 51% in sample LM.

Figure 7b shows the $^4He/^{20}Ne$ ratios versus the DOC/DIC ratios. The ^{14}C and minimum ^3H ages are reported for the corresponding samples. The trendline in Fig.7b, showing a relationship between the $^4He/^{20}Ne$ and the ratio between DOC and DIC, confirms the hypothesis of progressive mixing between surface groundwaters, where the dominant C source is organic matter, and deep geothermal waters, where the main C source is likely volcanic CO_2 and possibly C from carbonate dissolution. It is worth noting that the ages and temperatures of the waters decrease from 17,520±93 BP and 93˚C to ≥ 70 yrs and 65˚C along the trendline, further supporting this hypothesis.

4.6. Fluid circulation model at Copahue

By combining the structural information available for the study area with isotopic data from this study and from Roulleau et al. (2016), a conceptual model of fluid circulation in the CCVC is presented in Fig. 8.

The recent study of Lundgren et al. (2017), combining InSAR and seismic data collected during the 2011-2016 period of unrest, proposes the presence of two magma sources beneath Copahue volcano, with different degrees of magma differentiation (Cannatelli et al., 2016). The shallow source is located 2.5 km beneath the surface and is centered under the volcanic edifice. The second source is deeper, located 7-10 km below the surface and extending northeast, under the center of the Caviahue caldera (Fig. 8).

The CCVC fluid composition is essentially dominated by the mixing between two components: the deep seated magmatic/hydrothermal fluids and the shallow groundwater system. The deep-seated fluids are degassing from the two magmatic sources identified below the volcanic/hydrothermal system. Helium isotopes provide a reliable tool to separate the two members of the deep signal, whereas the water chemical composition and the other isotopes presented in this study provide the opportunity to disentangle the deep signal from the shallow groundwater input. The main structures in the Caviahue caldera are NE-striking normal faults, resulting in a horst-and-graben setting, and NW-striking strike-slip faults, interpreted as accommodation zones between the main extensional structures (Lamberti et al., 2019). These sets of faults control the hydrothermal activity and CO_2 degassing in the CCVC (Chiodini et al., 2015; Roulleau et al., 2017; Lamberti et al., 2019). The TC, LM, LMM, and CB hydrothermal areas show helium ratios of up to 8.35Ra and higher CO_2 flux than AF and CC (Chiodini et al., 2015; Roulleau et al., 2016, 2017; Lamberti et al., 2019). These characteristics suggest independent fluid pathways and sources for AF-CC and TC-LM-LMM-CB hydrothermal areas (Barcelona et al., 2020). The hydrothermal zones of LM, LMM, CB, and TC are spatially associated with damage zones, related to the interaction of main deep-rooted NE-SW and NW-SE normal faults (Fig. 8), presenting a high density of fractures, high dilatational tendency, and high vertical permeability (Melnick et al., 2006; Lamberti et al., 2019; Barcelona et al., 2020). These faults generate a preferential zone, which allows the ascent of hydrothermal fluids from the deeper magmatic reservoir to the surface. The thermal springs LMM and CB, lie on the same NW-SE normal fault (Figure 8), despite showing mantle-derived helium isotopes and stable water isotopes of magmatic origin, present evidence of mixing with meteoric water at the surface, perhaps due to local variation in the thickness of the groundwater aquifer, with which the hydrothermal fluids interact during their ascent to the surface. Both LMM and CB samples present the highest concentration of silica and the tritium activity indicates water residence time >70 years, which represents the minimum age for the meteoric recharge. It suggests that, nevertheless the water composition is affected by a significant meteoric water component, the water circulation patterns are more complex and deeper than previously proposed.

The AF and CC hydrothermal zones, located closer to the volcanic edifice, are spatially associated with shallower sets of NE-SW- and NW-SE-oriented normal faults respectively (Melnick et a., 2006; Lamberti et al., 2019; Barcelona et al., 2020). These shallower sets of faults likely represent the escape route for the hydrothermal fluids exsolved from the shallow magmatic reservoir (Lundgren et al., 2017), presenting a lower $^{3}He/^{4}He$ ratio. The hydrothermal fluids separated from more evolved magmas, stored at shallow depths, present lower helium ratios due magma chamber degassing of the original mantle component combined with radiogenic ingrowth of ^{4}He within the magma and assimilation of country rock rich in ^{4}He (Hilton et al., 1993; Hilton et al., 2002; Tardani et al., 2016). The assimilation of radiogenic helium from country rocks, representing the basement of the Quaternary volcanic edifices, has been previously identified in Chilean Andes and exert a first order control on helium signatures in the magmatic sources and fumaroles, which in turn is controlled by the structural contexts (Tardani et al., 2016; Veloso et al., 2020; Rubidoux et al., 2020). Strontium isotopes, stable isotopes of water and $^{4}He/^{20}Ne$ ratio for AF sample show that the water is largely dominated by a significant meteoric water contribution in this area, which is consistent with the location, in the same area, of the groundwater recharge zone. The COP-2 borehole intercepts the vapor-dominated geothermal reservoir at 1400 m depth, and presents a helium ratio of 6.4Ra (Fig. 8). The $^{87}Sr/^{86}Sr$ ratio for COP-2 sample shows a significant deviation from those of the Quaternary volcanic products of the CCVC, indicating the presence of a radiogenic Sr source possibly from deeper-seated granitoids or from the Mesozoic sedimentary basement, which is in agreement with the presence of radiogenic helium.

6. CONCLUSIONS

The proposed hydrological model of Copahue, including two sources of deep volatiles (Fig. 8), can explain the spatial distribution of helium isotopes in the CCVC, including the INSAR and petrological data related to the magmatic sources in addition to the mapped and inferred structural features in the area.

The main results of this study are the absence of young water, both in the reservoir (COP-2 sample) and in the hydrological circuit feeding the shallow geothermal pools. The absence of tritium and minimum ^{14}C age estimates of 13-14ka suggest that the hydrological circuit is more complex than previously assumed (e.g., Agusto and Varekamp, 2016). This can have particular consequences either for the exploitation of the shallow circuit for thermal balneation in the Copahue Village and for the future exploitation of the field, for electricity production. The absence of tritium in shallow hot springs indicate that the average residence time is higher than 70 years and thus any future plan of balneotherapy expansion in the area need to take into account that recharge can be slower than estimated, limiting the use - on the long term - for larger recreational activities. The minimum ^{14}C residence time of 13-14ka suggest the presence of old waters together with the meteoric recharge from the summit of the Copahue. The occurrence of old fluids is not new in geothermal fields (e,.g., Pinti et al., 2019) but need to be taken into account and counterbalanced with a thoughtful plan of reinjection in case of future large-scale steam exploitation for electricity production.

Acknowledgements

This study was funded by the ANID-FONDAP project 15090013 “Centro de Excelencia en Geotermia de los Andes”, CEGA. Additional funding was provided by ANID-FONDECYT Iniciación grant #11130351 and ANID-FONDECYT Regular grant #1201219. We wish to thank the ANID-FONDEQUIP project EQM120098 for the trace element data obtained using the iCap

Q-ICP-MS equipment and Verónica Rodriguez and Erika Rojas at University of Chile for the fluid chemical data acquisition. The authors thank A. Poirier, J.-F. Hélie, A. Valadez, and L. Richard at GEOTOP for analyses of Sr, stable isotopes of water and CO_2, and noble gas isotopes, and for handling of samples for ^{14}C analysis. The authors also thank the “Ente Provincial Termas del Neuquén” who granted permission to take samples for this study.

References

Aggarwal, P. K., Araguas-Araguas, L., Choudhry, M., van Duren, M., Froehlich, K., 2014. Lower groundwater ^{14}C age by atmospheric CO$_2$ uptake during sampling and analysis. Groundwater 52, 20-24.

Agusto, M., Varekamp, J., 2016. The Copahue Volcanic-Hydrothermal System and Applications for Volcanic Surveillance, in: Tassi, F., Vaselli, O., Caselli, A.T. (Eds.), Copahue Volcano. Springer Berlin Heidelberg, Berlin, Heidelberg, pp. 199-238.

Agusto, M., Tassi, F., Caselli, A. T., Vaselli, O., Rouwet, D., Capaccioni, B., Caliro, S., Chiodini, G., Darrah, T., 2013. Gas geochemistry of the magmatic-hydrothermal fluid reservoir in the Copahue–Caviahue Volcanic Complex (Argentina). J. Volcanol. Geotherm. Res. 257, 44–56.

Allègre, C.J., Moreira, M., Staudacher, T., 1995. ^{4}He/^{3}He dispersion and mantle convection. Geophys. Res. Lett. 22, 2325-2328.

Barcelona, H., Yagupsky, D., Vigide, N., Senger, M., 2019. Structural model and slip-dilation tendency analysis at the Copahue geothermal system: Inferences on the reservoir geometry. J. Volcanol. Geotherm. Res. 375, 18-31.

Barcelona, H., Maffucci, R., Yagupsky, D., Senger, M., Bigi, S., 2020. Discrete fracture network model of the vapor zone leakages at the Copahue geothermal field. J. Struct. Geol. 140, 104155.

Benson, B.B., Krause Jr., D., 1980. Isotopic fractionation of helium during solution: a probe for the liquid state. J. Solut. Chem. 9, 895–909.

Birkle, P., Merkel, B., Portugal, E., Torres-Alvarado, I. S., 2001. The origin of reservoir fluids in the geothermal field of Los Azufres, Mexico: Isotopical and hydrological indications. Appl. Geochem. 16, 1595-1610.

Birkle, P., Portugal Marín, E., Pinti, D.L., Castro, M.C., 2016. Origin and evolution of geothermal fluids from Las Tres Vírgenes and Cerro Prieto fields, Mexico - Co-genetic volcanic activity and paleoclimatic constraints. Appl. Geochem. 65, 36-53.

Bonali F.L., Corazzato C., Bellotti F., Groppelli G., 2016. Active tectonics and its interactions with Copahue Volcano. In: Tassi F., Vaselli O., Caselli A. (eds) Copahue Volcano. Active Volcanoes of the World. Springer, Berlin, Heidelberg https://doi.org/10.1007/978-3-662-48005-2_2

Bowen, G.J., 2017. The online isotopes in precipitation calculator, v. 3.1, http://wateriso.utah.edu/waterisotopes/pages/data_access/oipc.html.

Cannatelli, C., Aracena, C., Leisen, M., Moncada, D., Roulleau, E., Vinet, N., Petrelli, M., Paolillo, A., Barra, F., Morata, D., 2016. Magma evolution at Copahue volcano (Chile/Argentina border): insights from melt inclusions. AGU Fall Meeting (Abstr.), 2016AGUFM.V31A3085C.

Chiodini, G., Allard, P., Caliro, S., Parello, F., 2000. ^{18}O exchange between steam and carbon dioxide in volcanic and hydrothermal gases: implications for the source of water. Geochim. Cosmochim. Acta 64, 2479-2488.

Chiodini, G., Cardellini, C., Lamberti, M., Agusto, M., Caselli, A., Liccioli, C., Caliro, S., 2015. Carbon dioxide diffuse emission and thermal energy release from hydrothermal systems at Copahue–Caviahue Volcanic Complex (Argentina). J. Volcanol. Geotherm. Res. 304, 294-303.

Craig, H., Lupton, J. E., Horibe, Y., 1978. A mantle helium component in Circum-Pacific volcanic gases: Hakone, the Marianas, and Mr. Lassen. In: Alexander, Ozima, M. (Eds.), Terrestrial Rare Gases. Advances in Earth and Planetary Science. Academic Publication, Japan, pp. 3–16.

Crann, C.A., Murseli, S., St-Jean, G., Zhao, X., Clark, I.D., Kieser, W.E., 2017. First status report on radiocarbon sample preparation at the A.E. Lalonde AMS Laboratory (Ottawa, Canada). Radiocarbon 59, 695–704.

Fournier, R. O., Truesdell, A. H., 1970. Chemical indicators of subsurface temperature applied to hot spring waters of Yellowstone National Park, Wyoming, USA. Geothermics 2, 529- 535.

Friedman, I., J.R. O'Neil 1977: Compilation of stable isotope fractionation factors of geochemical interest. – In: Data of Geochemistry 6th, Geol. Surv. Prof. Paper 440–KK, p. 61.

Giggenbach, W.F., Stewart, M.K., 1982. Processes controlling the isotopic composition of steam and water discharges from steam vents and steam-heated pools in geothermal areas. Geothermics 11, 71–80.

Giggenbach, W. F., Goguel, R. L., 1989. Methods for the collection and analysis of geothermal and volcanic water and gas samples. Department of Scientific and Industrial Research, Chemistry Division. Petone, New Zealand.

Gizaw, B., 1996. The origin of high bicarbonate and fluoride concentrations in waters of the Main Ethiopian Rift Valley, East African Rift system. J. Afr. Earth Sci. 22, 391-402.

Goff, F., Janik, C. J., 2000. Geothermal systems. Encyclopedia of volcanoes, John Wiley & Son, 817-834.

Goff, F., McMurtry, G.M., 2000. Tritium and stable isotopes of magmatic waters. J. Volcanol. Geotherm. Res. 97, 347-396.

Heemskerk, A. R., Johnson, J., 1998. Tritium analysis: technical procedure 1.0. University of Waterloo, Waterloo, ON.

Hilton D. R., Hammerschmidt K., Teufel S., Friedrichsen H., 1993. Helium isotope characteristics of Andean geothermal fluids and lavas. Earth Planet. Sci. Lett. 120, 265–282.

Hilton D. R., Fischer T. P., Marty B., 2002. Noble gases and volatile recycling at subduction zones. Rev. Mineral. Geochem.47, 319–370.

Karolytė, R., Serno, S., Johnson, G., Gilfillan, S.M.V., 2017. The influence of oxygen isotope exchange between CO_2 and H_2O in natural CO_2-rich spring waters: Implications for geothermometry. Appl. Geochem. 84, 173-186.

Kitaoka, K., 1990. Water circulation rates in a geothermal field: a study of tritium in the Beppu hydrothermal system, Japan. Geothermics 19, 515-539.

Javoy, M., Pineau, F., Delorme, H., 1986. Carbon and nitrogen isotopes in the mantle. Chem. Geol. 57, 41-62.

JICA, 1992. The feasibility study on the northern Neuquen geothermal development project. Japan International Cooperation Agency, Neuquen, p. 444.

Lamberti, M. C., Vigide, N., Venturi, S., Agusto, M., Yagupsky, D., Winocur, D., Barcelona, H., Velez, M., Cardellini, Tassi, F., 2019. Structural architecture releasing deep-sourced carbon dioxide diffuse degassing at the Caviahue–Copahue Volcanic Complex. J. Volcanol. Geotherm. Res. 374, 131-141.

Linares, E., Ostera, H.A., Mas, L., 1999. Cronologia Potasio-Argon del conplejo efusivo Copahue–Caviahue, Provincia de Neuquen. Rev. Asoc. Geol. Argent. 54 (3), 240–247.

Lundgren, P., Nikkhoo, M. Samsonov, S.V., Milillo, P., Gil-Cruz, F., Lazo, J., 2017. Source model for the Copahue volcano magma plumbing system constrained by InSAR surface deformation observations, J. Geophys. Res.: Solid Earth 122, 5729–5747.

Mas, L.C., Mas, G.R., Bengochea, L, 2000. Heat flow of Copahue geothermal field; its relation with tectonic scheme. Proc. World Geother. Congr. Kyoto-Beppu, Japan, pp. 1419-1424.

Mas, G., Mas, L., Bengochea, L., 1995. Zeolite zoning in drill holes of the Copahue geothermal field, Neuquén, Argentina. Proc. World Geother. Congr.,1077-1081.

Mas, L.C., 2005. Present status of the Copahue geothermal project. Proc. World Geother. Congr., Antalya, Turkey, pp. 1–10.

Mason, E., Edmonds, M., Turchyn, A.V., 2017. Remobilization of crustal carbon may dominate volcanic arc emissions. Science 357, 290-294

Maydagan, L., Franchini, M., Chiaradia, M., Bouhier, V., Di Giuseppe, N., Rey, R., Dimieri, L.,

2016. Petrogenesis of Quebrada de la Mina and Altar North porphyries (Cordillera of San Juan, Argentina): Crustal assimilation and metallogenic implications. Geosci. Frontiers 8, doi:10.1016/j.gsf.2016.11.011.

Melnick, D., Folguera, A., Ramos, V. A., 2006. Structural control on arc volcanism: the Copahue-Agrio complex, South-Central Andes (37º50´S). J. South Am. Earth Sci. 22, 66–88.

Morata, D., Reich, M., Muñoz-Saez, C., Daniele, L., Rivera, G., Volpi, G., Ceccioni, M., Guidetti, G., Cappetti, G., 2019. Origin and age of fluids at the Cerro Pabellón geothermal system, Northern Chile. Proceedings 41st New Zealand Geothermal Workshop, 25-27 November 2019, Auckland, New Zealand.

Morrison P., Pine J., 1955. Radiogenic origin of the helium isotopes in rock. Ann. N Y Acad. Sci. 62, 71–92.

Nakanishi, S., Abe, M., Todaka, N., Yamada, M., Sierra, J., Gingins, M., Pedro, G., 1995. Copahue geothermal system, Argentina: study of a vapor-dominated reservoir. Proc. World Geother. Congr., Florence, Italy, pp. 18-31.

Notsu, K., Wakita, H., Nakamura, Y., 1991. Strontium isotopic composition of hot spring and mineral spring waters, Japan. Appl. Geochem. 6, 543-551.

Panarello, H.O., 2002. Características isotópicas y termodinámicas de reservorio del campo geotérmico Copahue-Caviahue, provincia del Neuquén. Rev. Asoc. Geol. Argentina 57, 182-194.

Panichi, C., Ferrara, G., Gonfiantini, R., 1977. Isotope geothermometry in the Larderello geothermal field. Geothermics 5, 81–88.

Pinti, D.L., Castro, M.C., López-Hernández, A., Hernández Hernández, M.A., Richard, L., Hall, C.M., Shouakar-Stash, O., Flores-Armenta, M., Rodríguez-Rodríguez, M.H., 2019. Cerro Prieto Geothermal Field (Baja California, Mexico) – A fossil system? Insights from a noble gas study. J. Volcanol. Geotherm. Res. 371, 32-45.

Reimer, P. J., Brown, T. A., Reimer, R. W., 2004. Discussion: reporting and calibration of post-bomb ^{14}C data. Radiocarbon 46, 1299-1304.

Richard, L., Pinti, D.L., Hélie, J.-F., Hernández, A.L., Shibata, T., Castro, M.C., Sano, Y., Shouakar-Stash, O., Sandoval-Medina, F., 2019. Variability of deep carbon sources in Mexican geothermal fluids. J. Volcanol. Geother. Res. 370, 1-12.

Richet, P., Bottinga, Y., Javoy, M., 1977. A Review of Hydrogen, Carbon, Nitrogen, Oxygen, Sulphur, and Chlorine Stable Isotope Fractionation Among Gaseous Molecules. Annu. Rev. Earth Planet. Sci. 5, 65–110.

Robidoux, P., Rizzo, A.L., Aguilera, F., Aiuppa, A., Artale, M., Liuzzo, M., Nazzari, M., Zummo, F., 2020. Petrological and noble gas features of Lascar and Lastarria volcanoes (Chile): Inferences on plumbing systems and mantle characteristics. Lithos 370-371.

Roulleau, E., Tardani, D., Sano, Y., Takahata, N., Vinet, N., Bravo, F., Muñoz, C., Sanchez, J., 2016. New insight from noble gas and stable isotopes of geothermal/hydrothermal fluids at Caviahue-Copahue Volcanic Complex: Boiling steam separation and water-rock interaction at shallow depth. J. Volcanol. Geotherm. Res. 328, 70-83.

Roulleau, E., Bravo, F., Pinti, D.L., Barde-Cabusson, S., Pizarro, M., Tardani, D., de la Cal, F., 2017. Structural controls on fluid circulation at the Caviahue-Copahue Volcanic Complex (CCVC) geothermal area (Chile-Argentina), revealed by soil CO_2 and temperature, self-potential, and helium isotopes. J. Volcanol. Geotherm. Res. 341, 104-118.

Roulleau, E., Tardani, D., Vlastelic, I., Vinet, N., Sanchez, J., Sano, Y., Takahata, N., 2018. Multi-element isotopic evolution of magmatic rocks from Caviahue-Copahue Volcanic Complex (Chile-Argentina): Involvement of mature slab recycled materials. Chem. Geol. 476, 370-388.

Rowe Jr., G.L., Brantley, S.L., Fernandez, J.F., Borgia, A., 1995. The chemical and hydrologic structure of Poás Volcano, Costa Rica. J. Volcanol. Geotherm. Res. 64, 233-267.

Sielfeld, G., Cembrano, J., Lara, L., 2017. Transtension driving volcano-edifice anatomy: Insights from Andean transverse-to-the-orogen tectonic domains. Quatern. Int. 438, 33-49.

Sierra, J.L., Pedro, G., D'Amore, F., Panarello, H., 1992. Reservoir characteristics of the vapor dominated geothermal field of Copahue, Neuquen, Argentina, as established by isotopic and geochemical techniques, International Atomic Energy Agency (IAEA), pp. 13-30.

Smith, S.P., Kennedy, B.M., 1983. The solubility of noble gases in water and NaCl brine. Geochim. Cosmochim. Acta 47, 503-515.

Stefánsson, A., Arnórsson, S., 2005. The geochemistry of As, Mo, Sb and W in natural geothermal waters, Iceland. Proc. World Geother. Congr., Antalaya, Turkey, pp. 1-7.

Stuiver, M., Polach, H.A., 1977. Discussion: reporting of ^{14}C data. Radiocarbon 19, 355–63.

Taran, Y., Zelenski, M., 2015. Systematics of water isotopic composition and chlorine content in arc-volcanic gases. Geol. Soc. London Spec. Publ. 410, 237-262.

Tassi, F., Agusto, M., Lamberti, C., Caselli, A., Pecoraino, G., Caponi, C., Vaselli, O., 2017. The 2012–2016 eruptive cycle at Copahue volcano (Argentina) versus the peripheral gas manifestations: hints from the chemical and isotopic features of fumarolic fluids. Bull. Volcanol. 79, 69.

Thorpe, R.S., Francis, P.W., Harmon, R.S., Moorbath, S.E., Windley, B.F., 1981. Andean andesites and crustal growth. Phil. Trans. Royal Soc. London Series A 301, 305-320.

Varekamp, J. C., DeMoor, J. M., Merrill, M. D., Colvin, A. S., Goss, A. R., 2006. Geochemistry and isotopic characteristics of the Caviahue–Copahue volcanic complex, Province of Neuquén, Argentina. Geol. Soc. America Spec. Paper 407, 317–342.

Veloso E., Tardani D., Elizalde D., Godoy B., Sánchez-Alfaro P., Aron F., Reich M., Morata D.A., 2020. Review of the geodynamic constraints on the development and evolution of geothermal systems in the Central Andean Volcanic Zone (18–28°Lat.S). Intern. Geol. Rev. 62, 1294-1318

FIGURE CAPTIONS

Figure 1. Structural map of the CCVC. Solid and dashed lines represent main faults from Melnick et al. (2006), Rojas Vera et al. (2009), Barcelona et al. (2019), and Lamberti et al. (2019). White circles and squares represent the locations of sampled hot springs and wells respectively. Gray circles represent the thermal springs located in the area, but not sampled as part of this study. AF: Anfiteatro; CB: Cabañita; CC: Chanco-có; LM: Las Máquinas; LMM: Las Maquinitas; PM: Pucón-Mahuida; TC: Termas de Copahue.

Figure 2. Sulfate contents versus trace element concentrations of Al (a), Fe (b), Mn (c), Rb (d), As (e) and Cs (f) for the well COP-2 condensate (blue square) and hot spring waters (blue circles).

Figure 3. Relationship between the 1000 ln α (CO_2–H_2O) in volcanic and hydrothermal fluids from the CCVC and their emission temperatures. The theoretical curves for equilibrium fractionation between CO_2 and H_2O in the gas phase from Friedman and O'Neil, (1977) and Richet et al. (1977), and the polynomial best fit representing the volcanic and hydrothermal fluids (Chiodini et al., 2000) are reported for comparison.

Figure 4. δ^2H versus (CO_2-corrected-) δ^{18}O of the CCVC sampled hot spring waters and COP-2 well condensate. The stable isotopic composition of geothermal pools (gray circles), local meteoric water line (LMWL) and evaporation line (EVAP) are from Agusto and Varekamp (2016). The andesitic water and magmatic water fields, as defined by Taran and Zelenski (2015), are also indicated, together with meteoric water endmember (green star; Panarello, 2002) and those calculated using OIPC at Copahue summit (light blue star) and at 1600m elevation (dark blue) (Agusto and Varekamp, 2016).

Figure 5. Strontium isotope ratios (^{87}Sr/^{86}Sr) versus the temperature of the sampled fluids (in °C) (a), SiO_2 contents (b) and the δ^{13}C-CO_2 (c). The orange area (labelled "local volcanics")

represents the range of measured $^{87}Sr/^{86}Sr$ values in local Copahue volcanic rocks (data from Varekamp et al., 2006 and Roulleau et al., 2018).

Figure 6. R/Ra versus $^{4}He/^{20}Ne$ of CCVC samples from this study and fumarole samples from Roulleau et al. (2016). The MORB, crust, Air and Air-Saturated Water (ASW) endmembers are reported. Dashed lines represent only mixing curves between mantle, crust, and ASW endmembers.

Figure 7. $^{4}He/^{20}Ne$ ratio versus $\delta^{2}H$ (a) and DOC/DIC ratio (b). The water ages measured using ^{14}C are reported for LM, COP-2, and TC samples.

Figure 8. Block model showing the structurally-controlled fluid circulation proposed for the CCVC. Black lines represent the main and secondary faults and fractures from Melnick et al. (2006), Rojas Vera et al. (2009), Barcelona et al. (2019), and Lamberti et al. (2019). The geometry and orientation of deep and shallow magmatic reservoirs are reported as proposed by Lundgren et al. (2017). The geothermal reservoir is reported as described by Barcelona et al. (2019). Blue, orange, and red arrows represent the ascent pathways of hydrothermal fluids with low (4.5 to 5.5 Ra), intermediate (5.6 to 6.9 Ra), and high helium (7.0 to 9.0 Ra) ratios respectively.

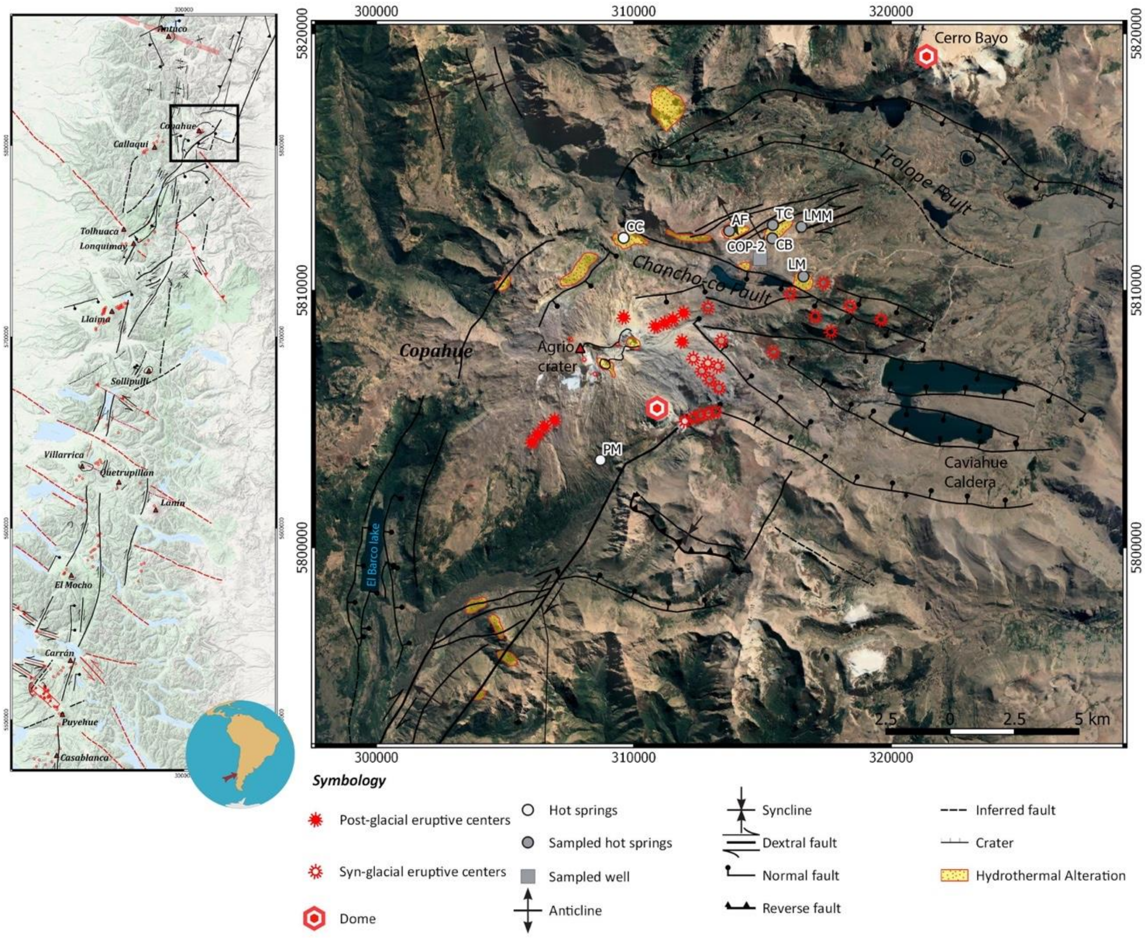

Antuco
Copahue
Callaqui
Tolhuaca
Lonquimay
Llaima
Sollipulli
Villarrica
Quetrupillan
Lanin
El Mocho
Carrán
Puyehue
Casablanca
300000
310000
320000
5820000
5810000
5800000
Cerro Bayo
Trolope Fault
Chancho-co Fault
CC
AF
TC
LMM
COP-2
CB
LM
Copahue
Agrio crater
PM
Caviahue Caldera
El Barco lake
2.5
0
2.5
5 km
Symbology
Post-glacial eruptive centers
Syn-glacial eruptive centers
Dome
Hot springs
Sampled hot springs
Sampled well
Anticline
Syncline
Dextral fault
Normal fault
Reverse fault
Inferred fault
Crater
Hydrothermal Alteration

Figure 1

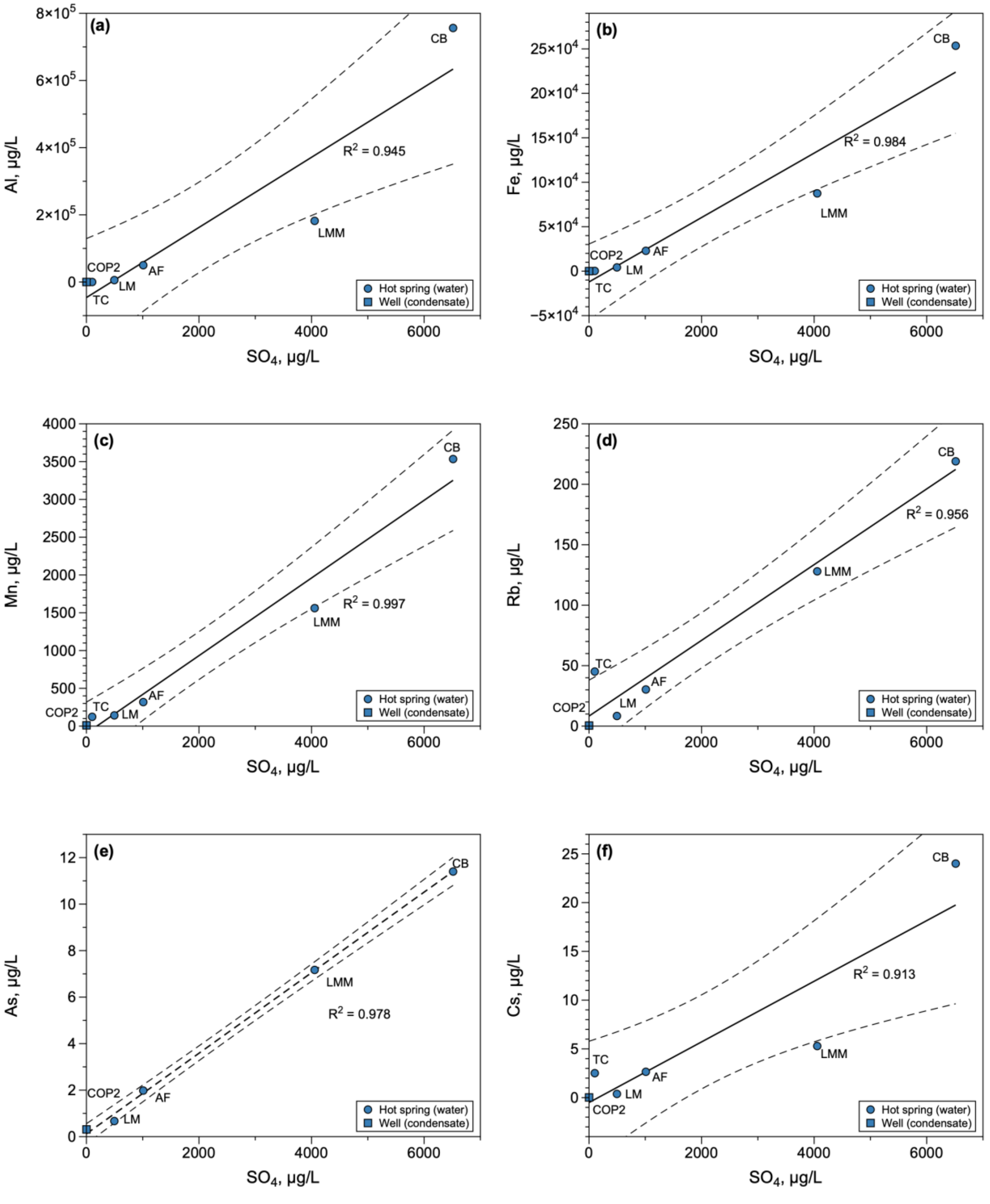
(a)
Al, µg/L
8×10^5
6×10^5
4×10^5
2×10^5
0
R^2 = 0.945
CB
LMM
AF
LM
COP2
TC
SO4, µg/L
0
2000
4000
6000
● Hot spring (water)
■ Well (condensate)
(b)
Fe, µg/L
25×10^4
20×10^4
15×10^4
10×10^4
5×10^4
0
−5×10^4
R^2 = 0.984
CB
LMM
AF
LM
COP2
TC
SO4, µg/L
● Hot spring (water)
■ Well (condensate)
(c)
Mn, µg/L
4000
3500
3000
2500
2000
1500
1000
500
0
R^2 = 0.997
CB
LMM
AF
TC
LM
COP2
SO4, µg/L
● Hot spring (water)
■ Well (condensate)
(d)
Rb, µg/L
250
200
150
100
50
0
R^2 = 0.956
CB
LMM
TC
AF
LM
COP2
SO4, µg/L
● Hot spring (water)
■ Well (condensate)
(e)
As, µg/L
12
10
8
6
4
2
0
R^2 = 0.978
CB
LMM
COP2
AF
LM
SO4, µg/L
● Hot spring (water)
■ Well (condensate)
(f)
Cs, µg/L
25
20
15
10
5
0
R^2 = 0.913
CB
LMM
TC
AF
LM
COP2
SO4, µg/L
● Hot spring (water)
■ Well (condensate)

Figure 2

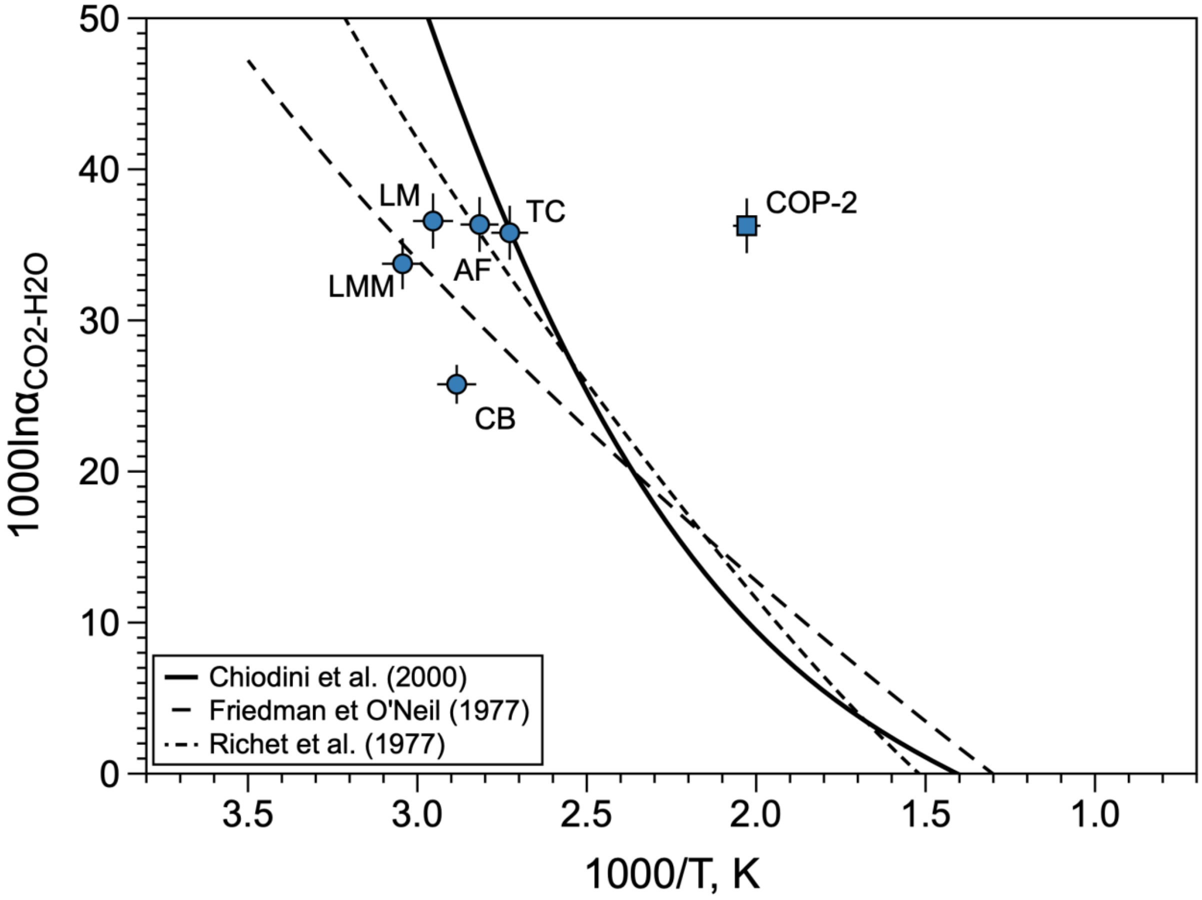
50
40
30
20
10
0
1000lnα$_{CO2-H2O}$
LM
TC
COP-2
LMM
AF
CB
Chiodini et al. (2000)
Friedman et O'Neil (1977)
Richet et al. (1977)
3.5
3.0
2.5
2.0
1.5
1.0
1000/T, K

Figure 3

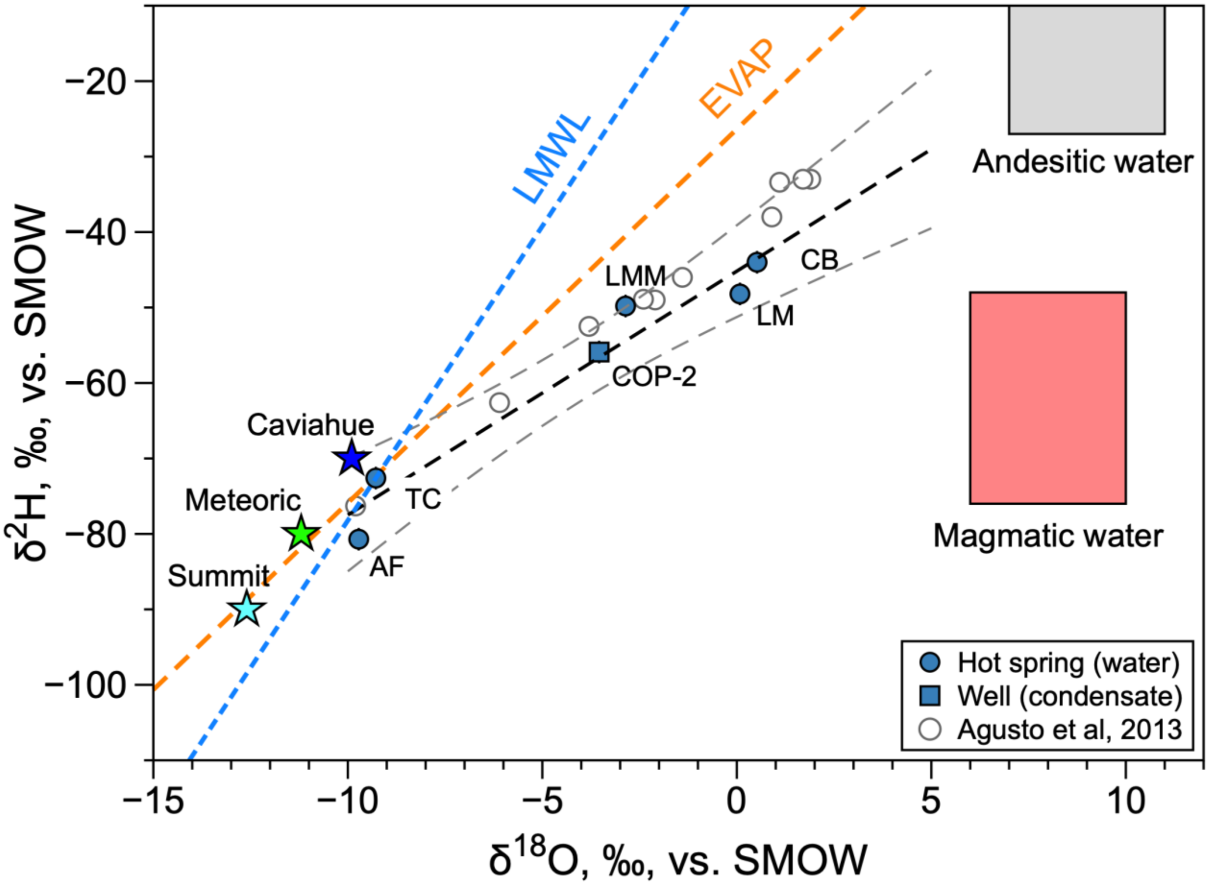

LMWL
EVAP
Andesitic water
Magmatic water
Caviahue
Meteoric
Summit
LMM
CB
LM
COP-2
TC
AF
● Hot spring (water)
■ Well (condensate)
○ Agusto et al, 2013
−20
−40
−60
−80
−100
−15
−10
−5
0
5
10
δ²H, ‰, vs. SMOW
δ¹⁸O, ‰, vs. SMOW

Figure 4

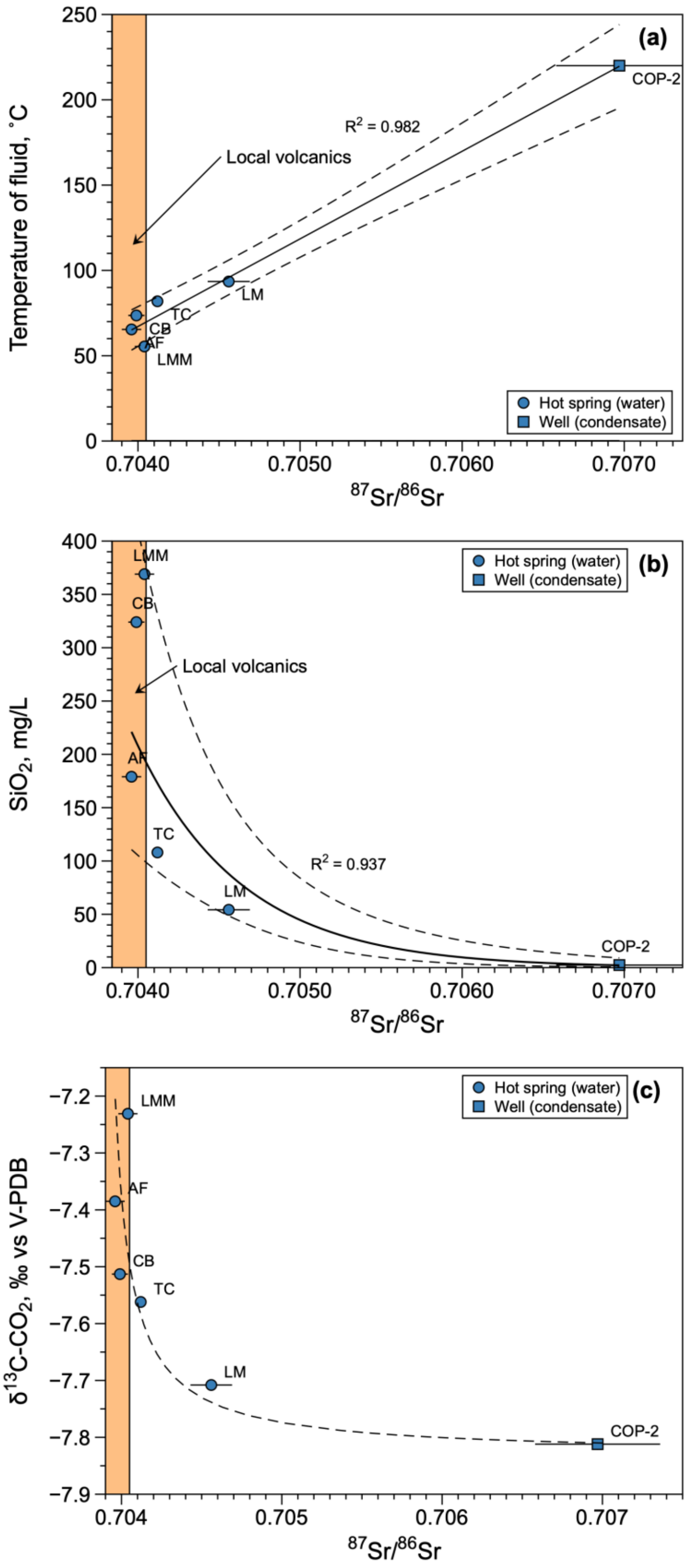
(a)
Temperature of fluid, ˚C
250
200
150
100
50
0
0.7040
0.7050
0.7060
0.7070
$^{87}Sr/^{86}Sr$
$R^2 = 0.982$
Local volcanics
COP-2
LM
TC
CB
AF
LMM
Hot spring (water)
Well (condensate)
(b)
SiO_2, mg/L
400
350
300
250
200
150
100
50
0
LMM
CB
Local volcanics
AF
TC
$R^2 = 0.937$
LM
COP-2
0.7040
0.7050
0.7060
0.7070
$^{87}Sr/^{86}Sr$
Hot spring (water)
Well (condensate)
(c)
$\delta^{13}C$-CO_2, ‰ vs V-PDB
−7.2
−7.3
−7.4
−7.5
−7.6
−7.7
−7.8
−7.9
LMM
AF
CB
TC
LM
COP-2
0.704
0.705
0.706
0.707
$^{87}Sr/^{86}Sr$
Hot spring (water)
Well (condensate)

Figure 5

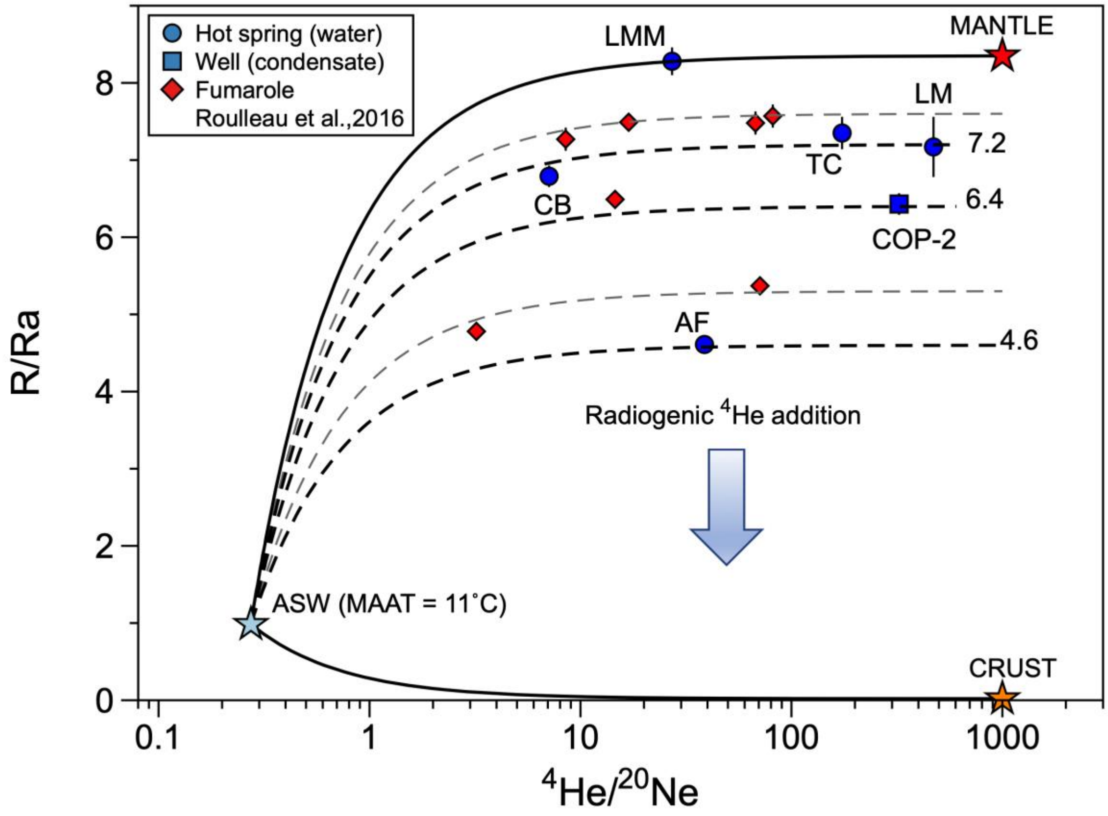
Hot spring (water)
Well (condensate)
Fumarole
Roulleau et al.,2016
LMM
MANTLE
LM
TC
CB
COP-2
AF
7.2
6.4
4.6
Radiogenic ^{4}He addition
ASW (MAAT = 11˚C)
CRUST
R/Ra
0
2
4
6
8
0.1
1
10
100
1000
^{4}He/^{20}Ne

Figure 6

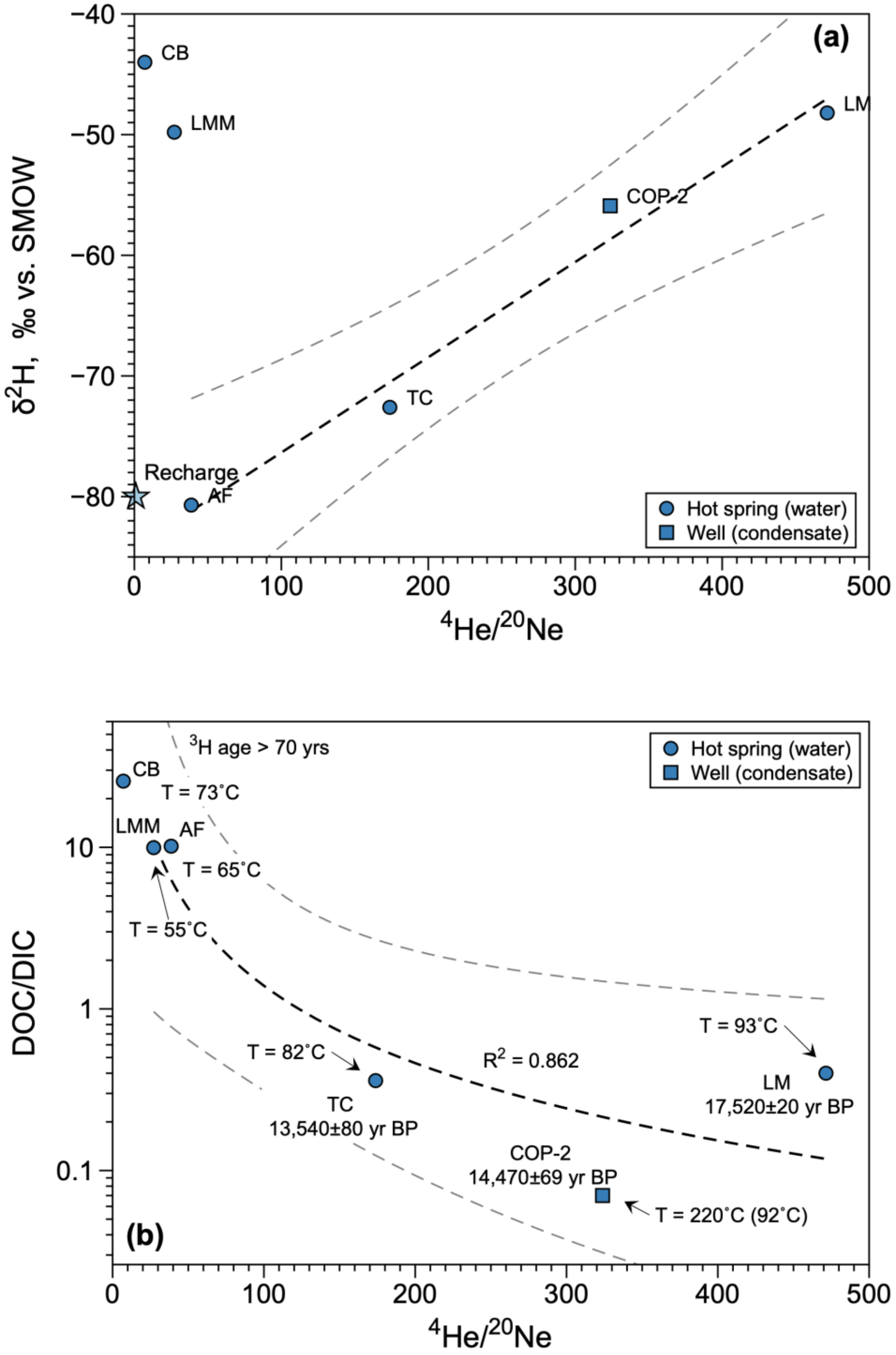
(a)
δ²H, ‰ vs. SMOW
⁴He/²⁰Ne
−40
−50
−60
−70
−80
0
100
200
300
400
500
CB
LMM
LM
COP-2
TC
Recharge
AF
Hot spring (water)
Well (condensate)
(b)
DOC/DIC
⁴He/²⁰Ne
10
1
0.1
0
100
200
300
400
500
³H age > 70 yrs
CB
T = 73˚C
LMM
AF
T = 65˚C
T = 55˚C
T = 82˚C
TC
13,540±80 yr BP
R² = 0.862
T = 93˚C
LM
17,520±20 yr BP
COP-2
14,470±69 yr BP
T = 220˚C (92˚C)
Hot spring (water)
Well (condensate)

Figure 7

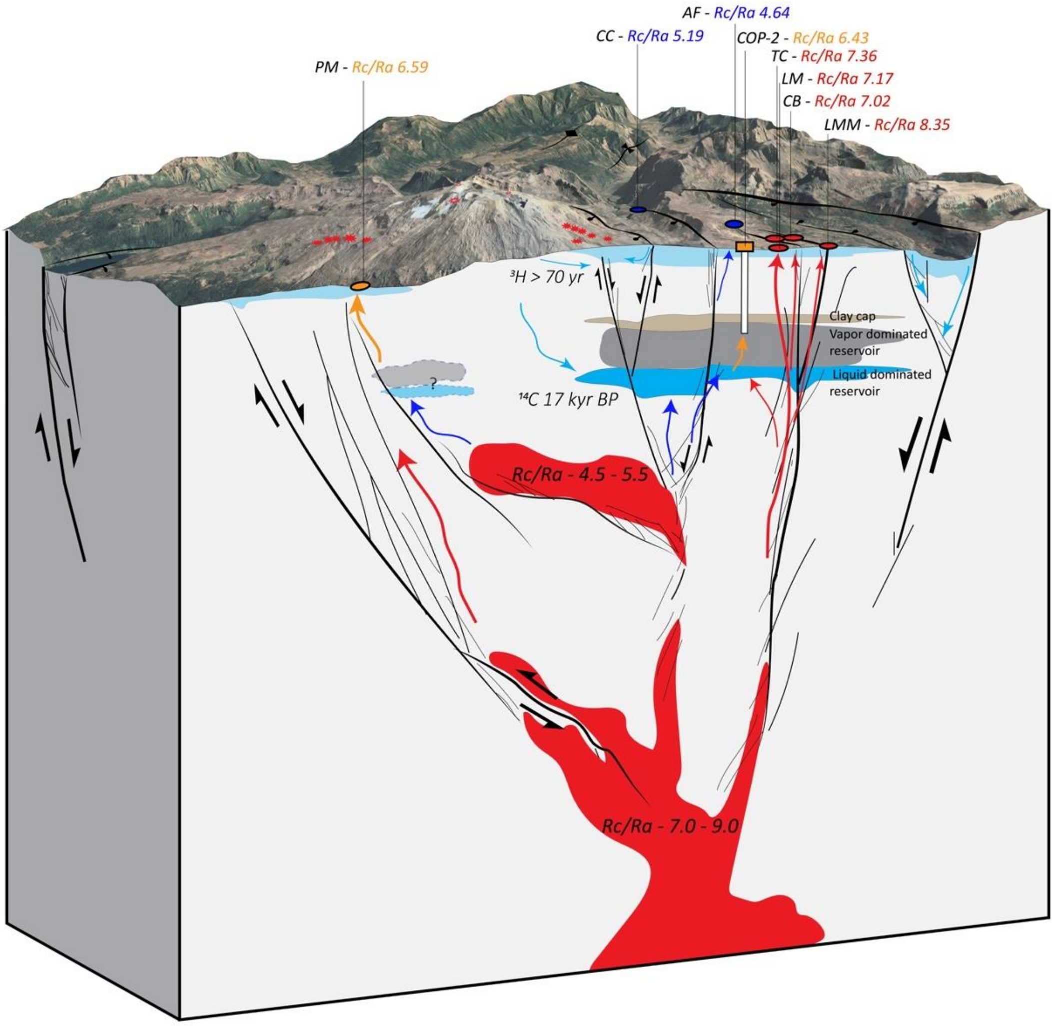
AF - Rc/Ra 4.64
CC - Rc/Ra 5.19
COP-2 - Rc/Ra 6.43
TC - Rc/Ra 7.36
PM - Rc/Ra 6.59
LM - Rc/Ra 7.17
CB - Rc/Ra 7.02
LMM - Rc/Ra 8.35
^{3}H > 70 yr
Clay cap
Vapor dominated reservoir
?
Liquid dominated reservoir
^{14}C 17 kyr BP
Rc/Ra - 4.5 - 5.5
Rc/Ra - 7.0 - 9.0

Figure 8

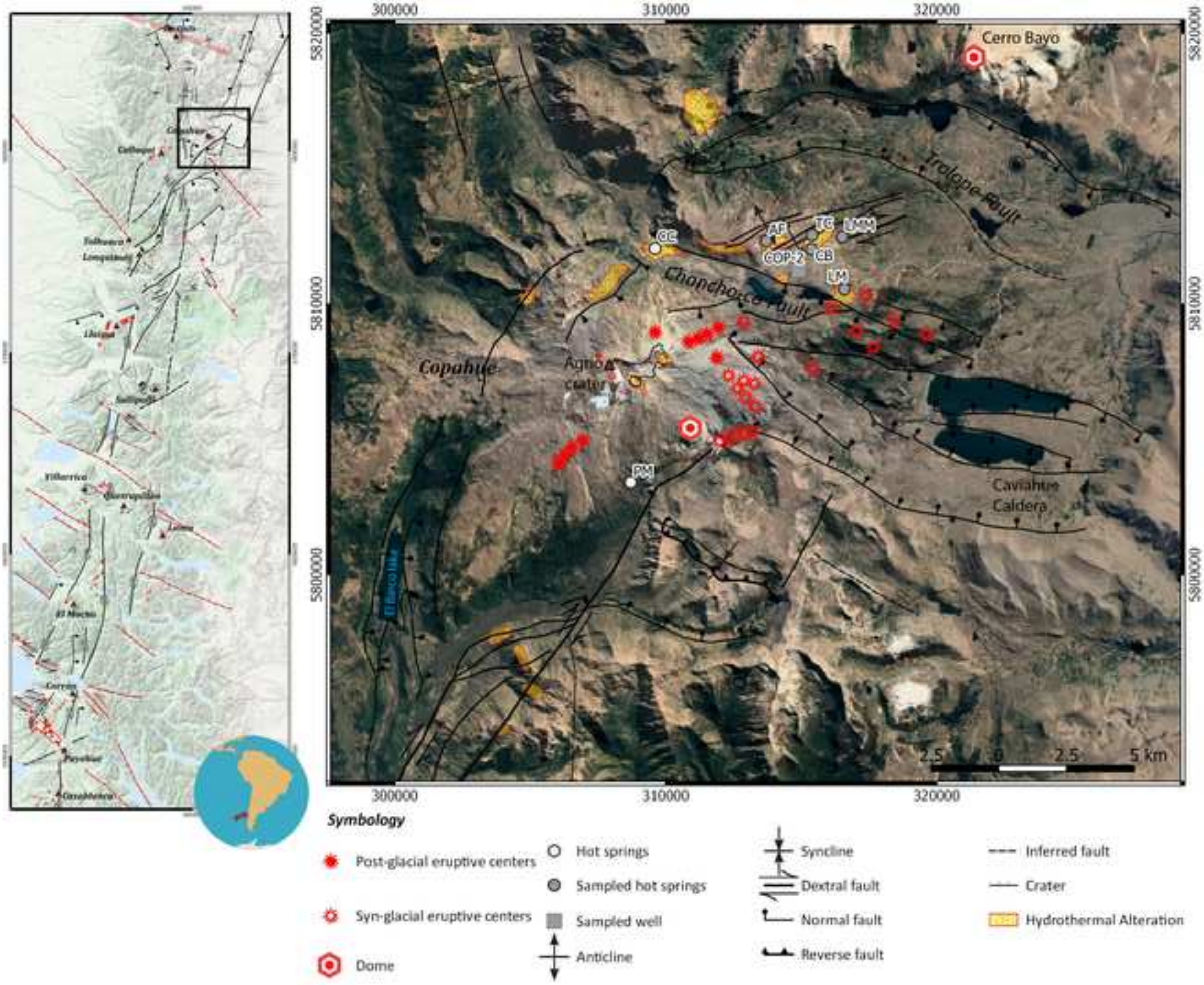
Copahue
Callaqui
Tolhuaca
Lonquimay
Llaima
Sollipulli
Villarrica
Quetrupillán
Lanín
El Mocho
Carrán
Puyehue
Casablanca
300000
310000
320000
5820000
5810000
5800000
Cerro Bayo
Trolope Fault
Chancho-co Fault
GC
AF
TC
LMM
COP-2
CB
LM
Copahue
Agrio crater
PM
Caviahue Caldera
El Barco Lake
2.5
0
2.5
5 km
Symbology
Post-glacial eruptive centers
Syn-glacial eruptive centers
Dome
Hot springs
Sampled hot springs
Sampled well
Anticline
Syncline
Dextral fault
Normal fault
Reverse fault
Inferred fault
Crater
Hydrothermal Alteration

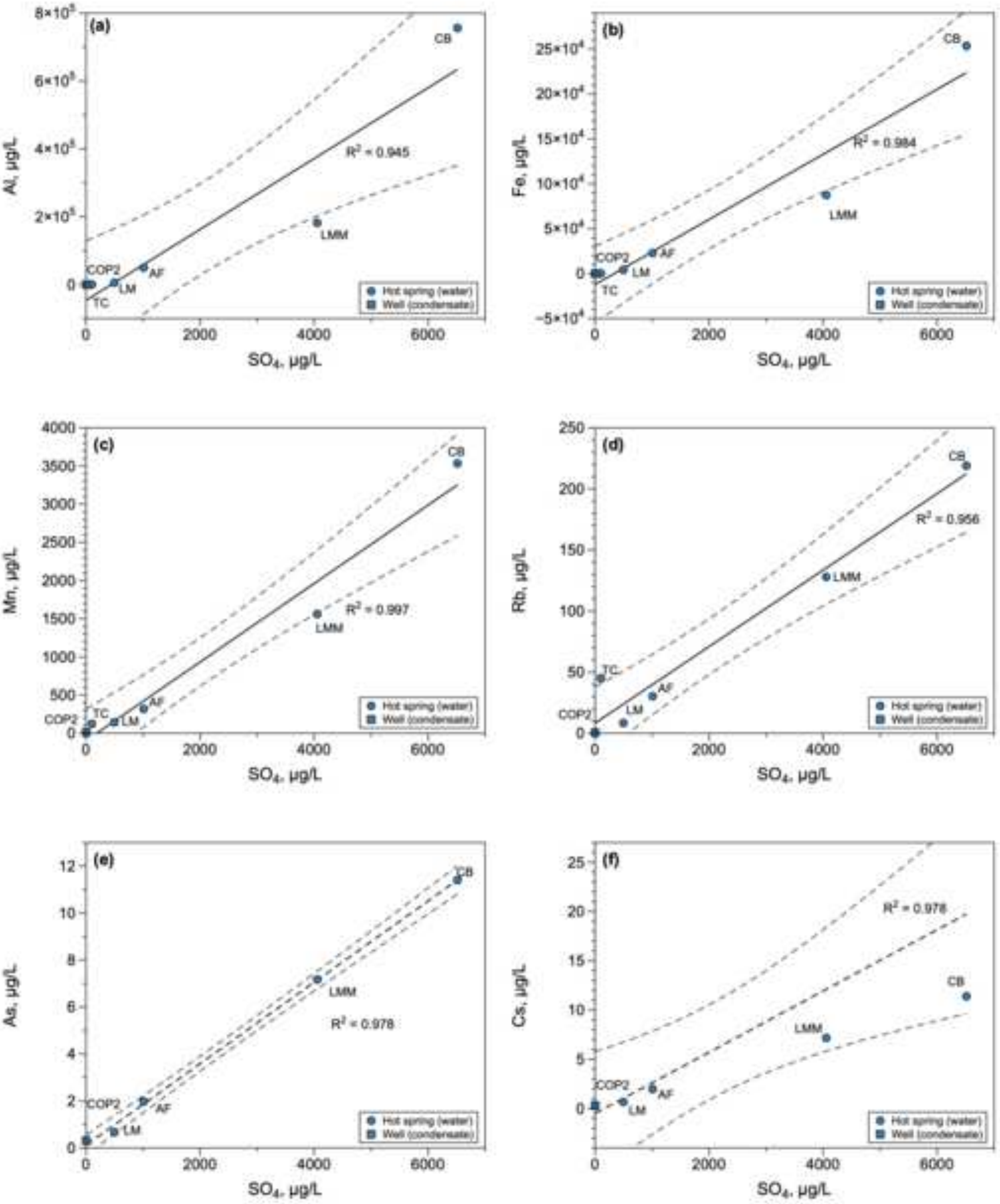
(a)
Al, µg/L
8×10⁵
6×10⁵
4×10⁵
2×10⁵
0
CB
R² = 0.945
LMM
COP2
AF
LM
TC
SO₄, µg/L
0
2000
4000
6000
Hot spring (water)
Well (condensate)
(b)
Fe, µg/L
25×10⁴
20×10⁴
15×10⁴
10×10⁴
5×10⁴
0
−5×10⁴
CB
R² = 0.984
LMM
COP2
AF
LM
TC
SO₄, µg/L
Hot spring (water)
Well (condensate)
(c)
Mn, µg/L
4000
3500
3000
2500
2000
1500
1000
500
0
CB
R² = 0.997
LMM
AF
TC
COP2
LM
SO₄, µg/L
Hot spring (water)
Well (condensate)
(d)
Rb, µg/L
250
200
150
100
50
0
CB
R² = 0.956
LMM
TC
AF
LM
COP2
SO₄, µg/L
Hot spring (water)
Well (condensate)
(e)
As, µg/L
12
10
8
6
4
2
0
CB
LMM
R² = 0.978
COP2
AF
LM
SO₄, µg/L
Hot spring (water)
Well (condensate)
(f)
Cs, µg/L
25
20
15
10
5
0
R² = 0.978
CB
LMM
COP2
AF
LM
SO₄, µg/L
Hot spring (water)
Well (condensate)

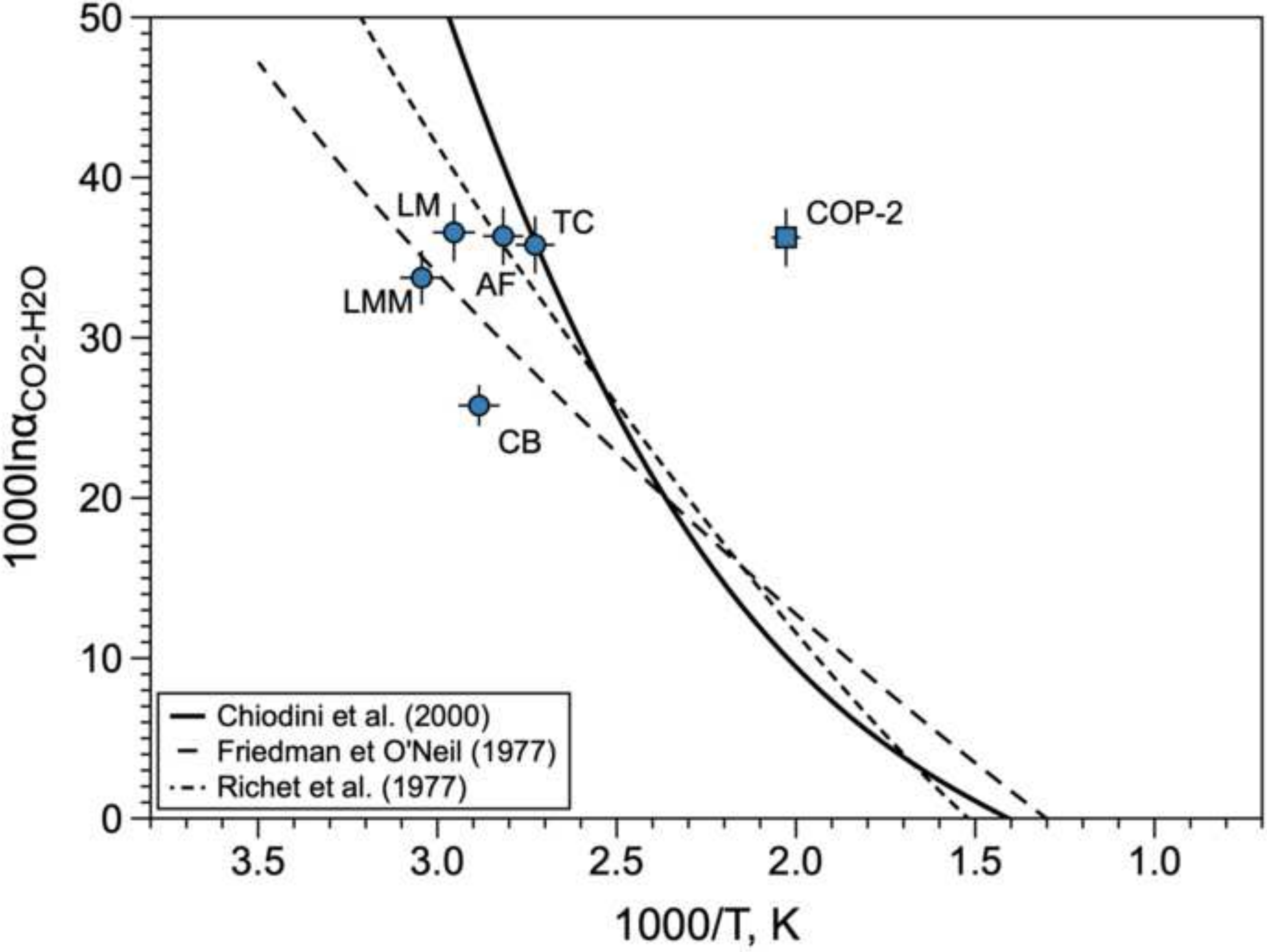
50
40
30
20
10
0
1000lnα$_{CO2-H2O}$
3.5
3.0
2.5
2.0
1.5
1.0
1000/T, K
LM
TC
COP-2
LMM
AF
CB
Chiodini et al. (2000)
Friedman et O'Neil (1977)
Richet et al. (1977)

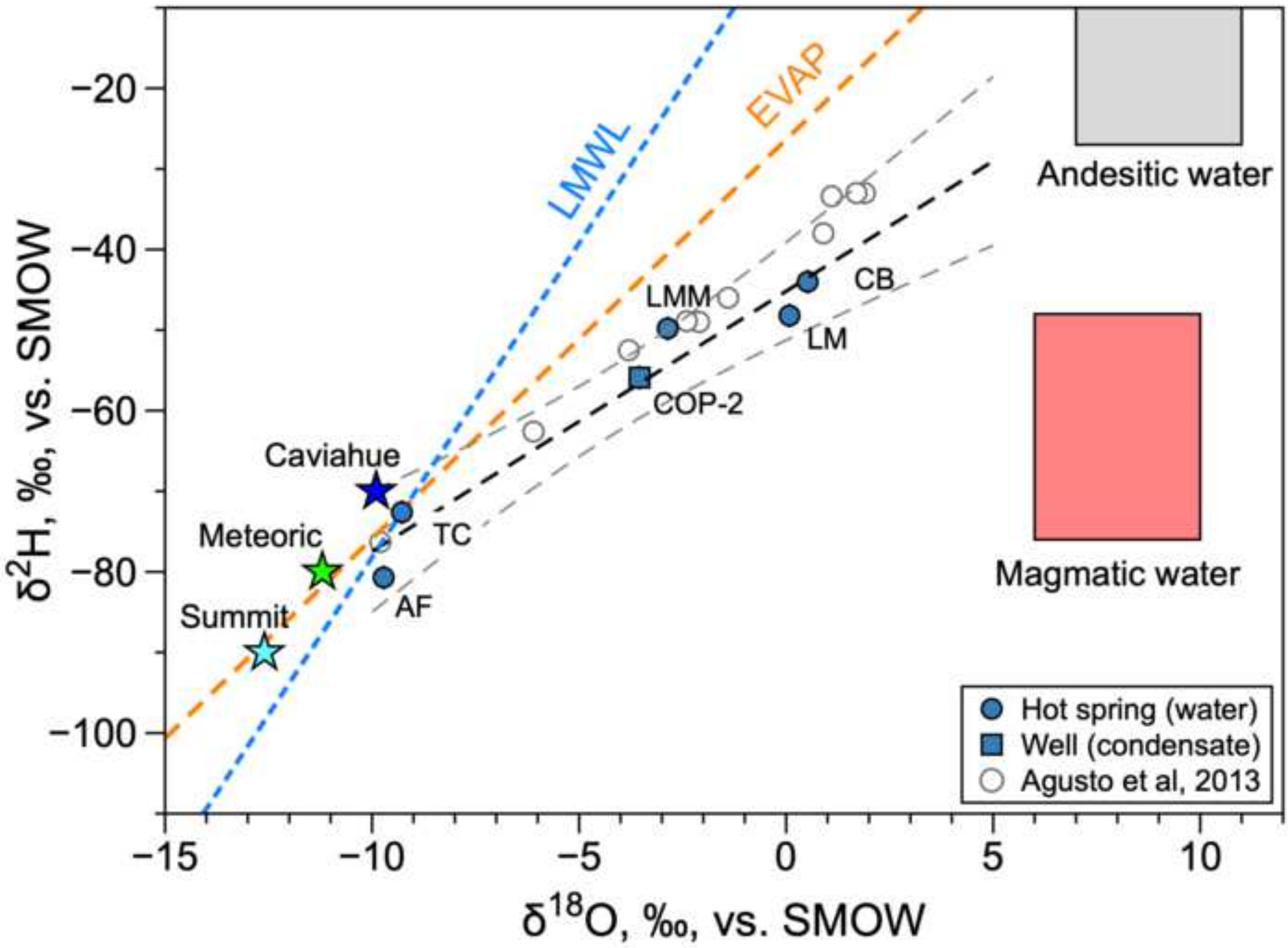
LMWL
EVAP
Andesitic water
Magmatic water
Caviahue
Meteoric
Summit
LMM
CB
LM
COP-2
TC
AF
● Hot spring (water)
■ Well (condensate)
○ Agusto et al, 2013
−20
−40
−60
−80
−100
δ2H, ‰, vs. SMOW
−15
−10
−5
0
5
10
δ18O, ‰, vs. SMOW

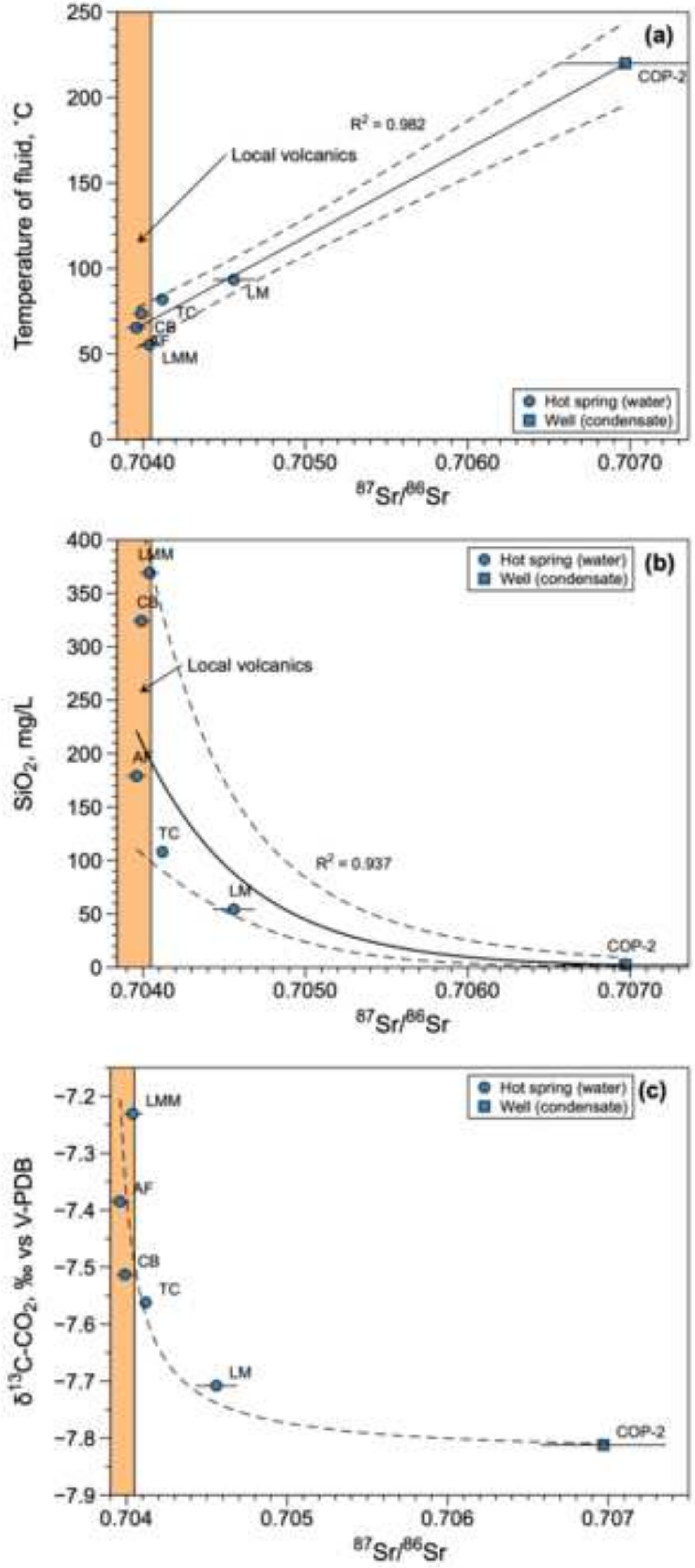
(a)
Temperature of fluid, °C
250
200
150
100
50
0
R² = 0.982
Local volcanics
COP-2
LM
TC
CB
AF
LMM
Hot spring (water)
Well (condensate)
0.7040
0.7050
0.7060
0.7070
87Sr/86Sr
(b)
SiO2, mg/L
400
350
300
250
200
150
100
50
0
LMM
CB
Local volcanics
AF
TC
R² = 0.937
LM
COP-2
Hot spring (water)
Well (condensate)
0.7040
0.7050
0.7060
0.7070
87Sr/86Sr
(c)
δ13C-CO2, ‰ vs V-PDB
−7.2
−7.3
−7.4
−7.5
−7.6
−7.7
−7.8
−7.9
LMM
AF
CB
TC
LM
COP-2
Hot spring (water)
Well (condensate)
0.704
0.705
0.706
0.707
87Sr/86Sr

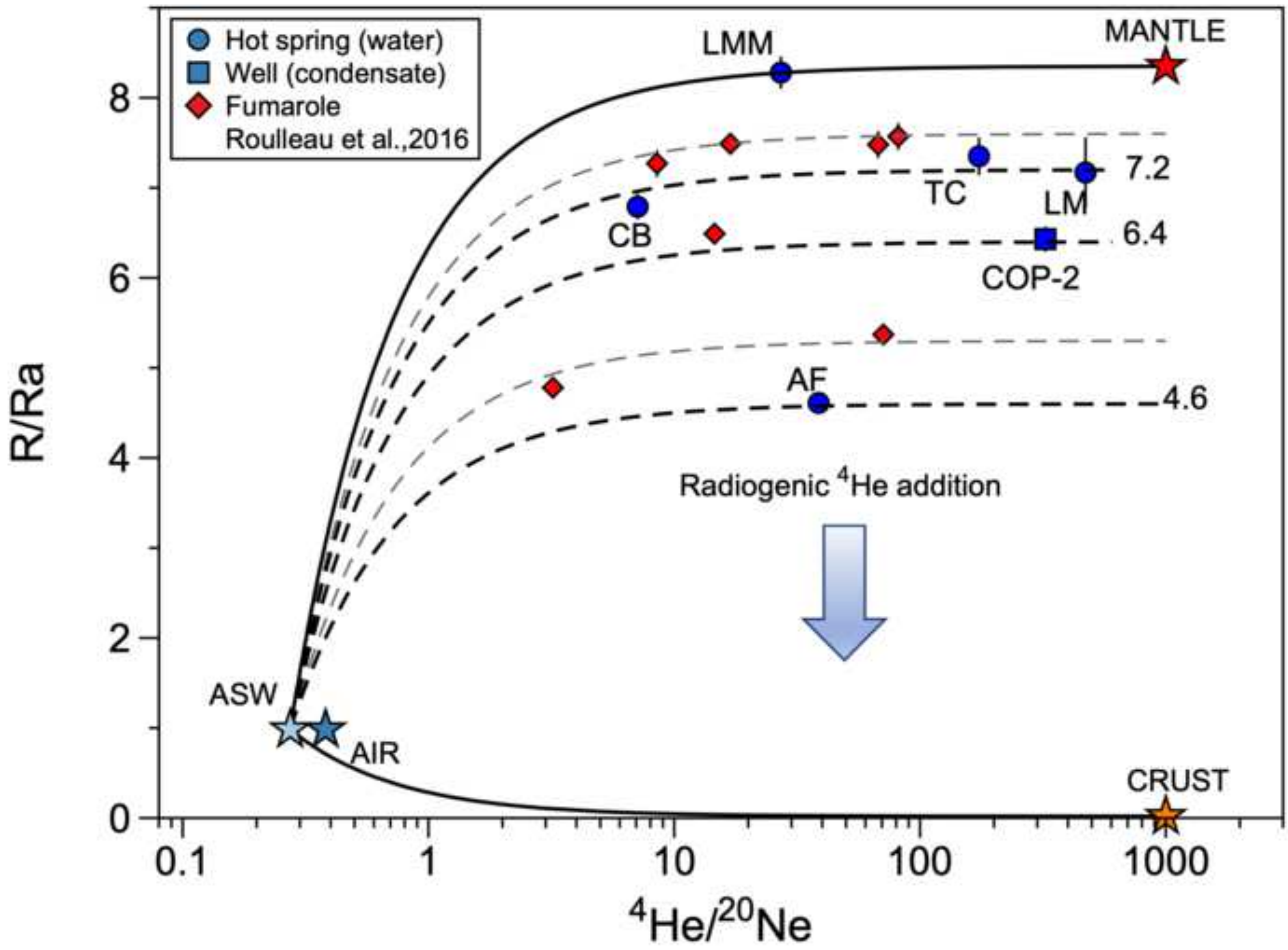
Hot spring (water)
Well (condensate)
Fumarole
Roulleau et al.,2016
LMM
MANTLE
TC
LM
7.2
CB
6.4
COP-2
AF
4.6
Radiogenic ^{4}He addition
ASW
AIR
CRUST
R/Ra
8
6
4
2
0
0.1
1
10
100
1000
^{4}He/^{20}Ne

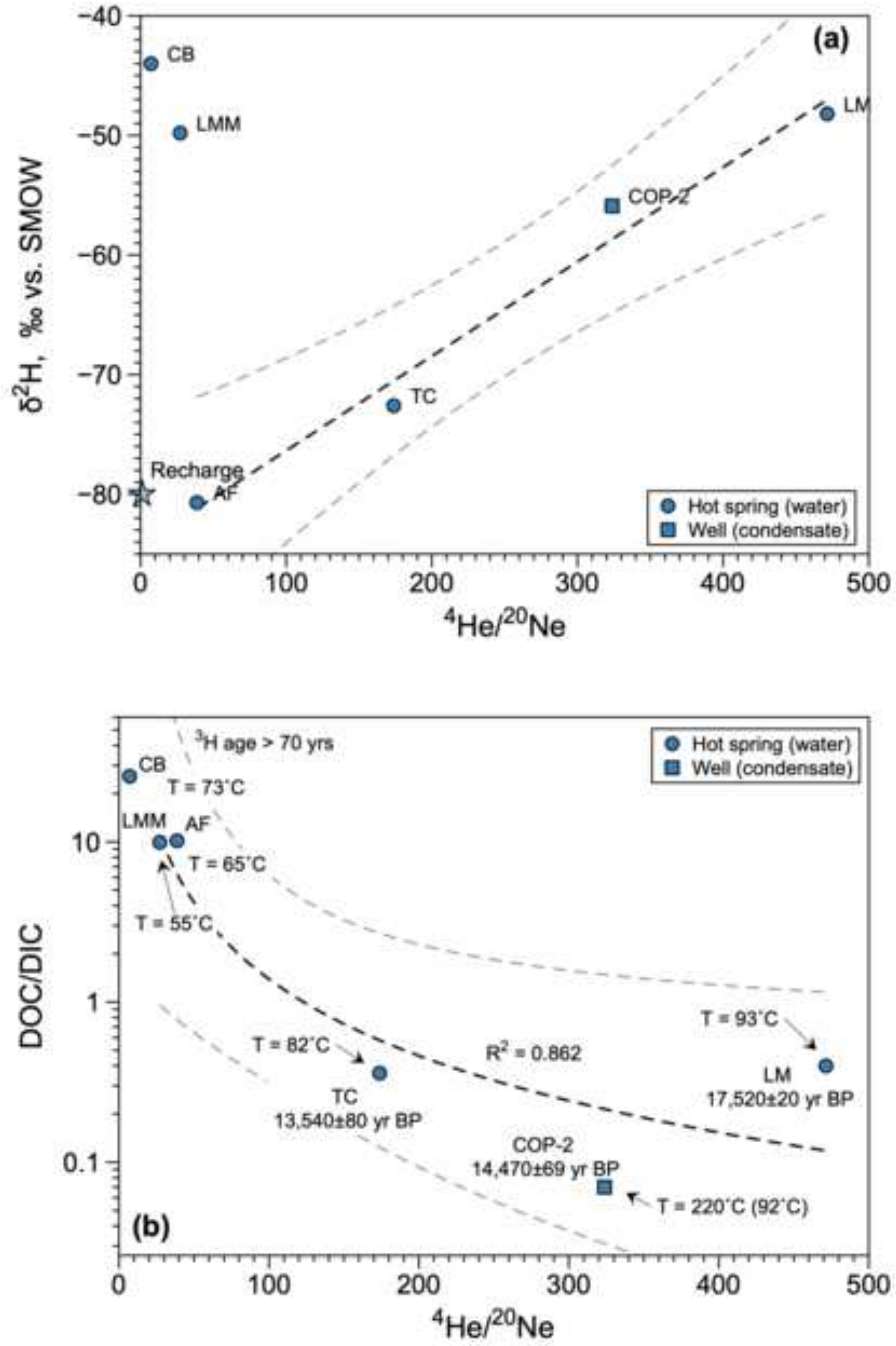
(a)
δ2H, ‰ vs. SMOW
4He/20Ne
−40
−50
−60
−70
−80
0
100
200
300
400
500
CB
LMM
LM
COP-2
TC
Recharge
AF
Hot spring (water)
Well (condensate)
(b)
DOC/DIC
4He/20Ne
10
1
0.1
0
100
200
300
400
500
3H age > 70 yrs
CB
T = 73°C
LMM
AF
T = 65°C
T = 55°C
T = 82°C
TC
13,540±80 yr BP
R2 = 0.862
T = 93°C
LM
17,520±20 yr BP
COP-2
14,470±69 yr BP
T = 220°C (92°C)
Hot spring (water)
Well (condensate)

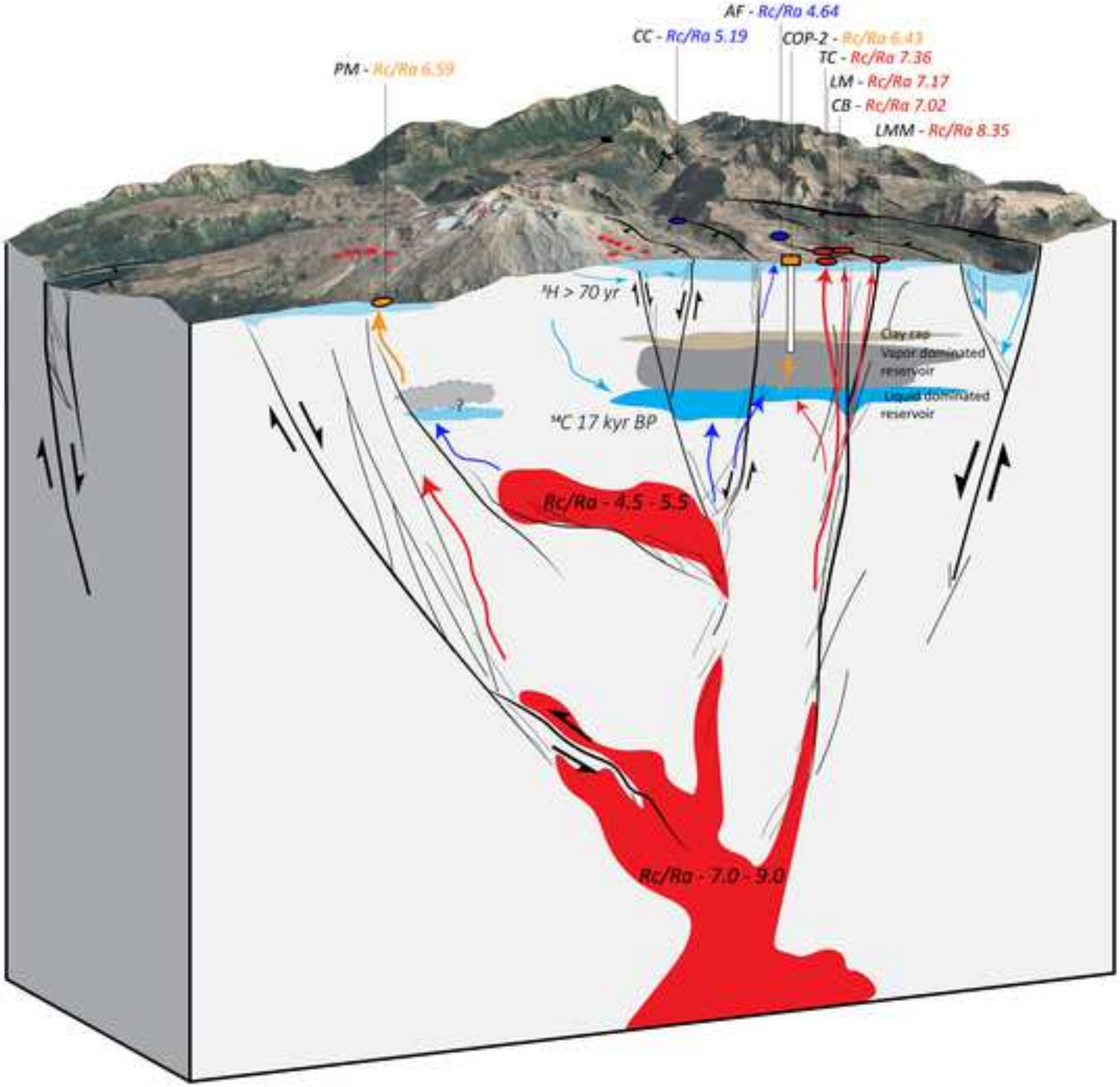
AF - Rc/Ra 4.64
CC - Rc/Ra 5.19
COP-2 - Rc/Ra 6.43
TC - Rc/Ra 7.36
LM - Rc/Ra 7.17
CB - Rc/Ra 7.02
LMM - Rc/Ra 8.35
PM - Rc/Ra 6.59
^{3}H > 70 yr
Clay cap
Vapor dominated reservoir
Liquid dominated reservoir
?
^{14}C 17 kyr BP
Rc/Ra - 4.5 - 5.5
Rc/Ra - 7.0 - 9.0

Table 1. Ionic concentrations in water and condensate samples from Copahue thermal area.

Sample	Location name	Type	Longitude E WG84, m	Latitude S WG84, m	Altitude m.s.l.	T ˚C	pH -
LM	Las Máquinas	Hot spring	316599	5810539	1979	93.5	2.26
TC	Termas Copahue	Hot spring	315412	5812554	2013	81.9	6.8
LMM	Las Maquinitas	Hot spring	316522	5812479	2021	55.4	1.9
AF	Anfiteatro	Hot spring	313708	5812321	2152	65.4	2.39
CB	Cabañita	Hot spring	315388	5812032	2055	73.6	2.21
COP-2	-	Well cond	314918	5811238	2075	92	8.5

Sample
LM
TC
LMM
AF
CB
COP-2

n.d. = not determined
IB = Ionic balance

Conductivity µS/cm	Na mg/L	Ca mg/L	Mg mg/L	K mg/L	Cl mg/L	HCO3 mg/L	CO3 mg/L	SO4 mg/L	SiO2 mg/L
	23.0	20.0	12.2	39.1	35.453	61	30	48	
2580	4.17	11.5	4.28	2.60	2.42	n.d.	n.d.	496	54.02
503	27.0	34.7	11.7	16.80	1.62	166.7	n.d.	102	108.0
11730	26.0	47.5	15.8	30.9	0.35	n.d.	n.d.	4055	369.0
3120	10.0	37.4	9.35	8.38	4.87	n.d.	n.d.	1010	179.0
12750	6.75	9.49	5.85	2.13	0.61	n.d.	n.d.	6515	324.0
79	1.24	0.201	0.043	0.43	0.90	33.3	2.5	0.81	2.40

	Fe mg/L	Al mg/L	Mn mg/L	Si mg/L	Li µg/L	Rb µg/L	Sr µg/L	Ba µg/L	Cs µg/L
	22.34	8.99	27	7					
	4.23	5.68	0.14	25.36	3.51	8.39	64.03	32.10	0.38
	0.24	0.03	0.12		31.40	45.10	245.00	70.90	2.51
	87.47	182.01	1.56	172.50	13.50	128.00	228.00	43.30	5.29
	22.88	50.01	0.32	83.68	6.00	30.30	374.00	68.70	2.65
	253.50	756.26	3.53	151.50	60.90	219.00	31.20	0.65	24.00
	0.03	0.03	0.01	1.12	0.09	0.48	0.73	0.29	0.02

F mg/L	B mg/L	IB %
18.99	3.6	
0.18	5.50	9.71
0.08	0.05	-6.24
0.66	0.51	-11.43
0.21	0.02	10.03
0.54	n.d.	-4.25
<0.03	0.001	-

As μg/L	Cr μg/L	Ni μg/L
0.67	1.67	1.53
n.d.	n.d.	0.86
7.17	23.70	8.20
1.98	37.50	7.39
11.40	88.30	33.60
0.31	4.27	0.59

Table 2. Isotopic composition of water, Sr, CO_2, He together with ^{3}H and ^{14}C activity in thermal wate

Sample	Type	δ^2H	±	δ^{18}O	±	δ^{18}O	δ^{13}C-CO_2	±	δ^{18}O-CO_2
		‰, SMOW		‰, SMOW		CO_2-corrected	‰, PDB		‰, PDB
LM	Hot spring	-48.2	1.5	0.08	0.10	0.08	-7.71	0.01	5.45
TC	Hot spring	-72.6	1.5	-9.17	0.10	-9.28	-7.56	0.01	-3.31
LMM	Hot spring	-49.8	1.5	-2.31	0.10	-2.86	-7.23	0.01	0.99
AF	Hot spring	-80.7	1.5	-9.72	0.10	-9.72	-7.39	0.01	-3.64
CB	Hot spring	-44.0	1.5	1.07	0.10	0.52	-7.51	0.01	-3.60
COP-2	Well	-55.9	1.5	-3.54	0.10	-3.54	-7.81	0.01	2.27

n.d. = not determined

rs of Copahue.

±	^{87}Sr/^{86}Sr	±	^{4}He/^{20}Ne	±	R/Ra	±	Rc/Ra	±	^{3}H TU	F(^{14}C)	±	^{14}C age yrs BP	±
0.05	0.70456	0.00013	471.46	14.14	7.17	0.39	7.17	0.42	n.d.	0.113	0.001	17520	93
0.02	0.70412	0.00003	173.83	5.21	7.35	0.21	7.36	0.26	n.d.	0.185	0.002	13540	80
0.05	0.70404	0.00006	27.17	0.82	8.28	0.18	8.37	0.25	0.80	n.d.	-	n.d.	-
0.02	0.70396	0.00006	38.70	1.16	4.61	0.10	4.64	0.14	n.d.	n.d.	-	n.d.	-
0.02	0.70399	0.00005	7.10	0.21	6.79	0.14	7.06	0.20	0.80	n.d.	-	n.d.	-
0.02	0.70697	0.00039	323.80	9.71	6.43	0.14	6.44	0.19	n.d.	0.165	0.001	14470	69

DIC ppm	DOC ppm
0.83	0.33
1.46	0.53
0.43	4.28
0.51	5.18
0.57	14.64
6.79	0.50

Conflict of Interest

Dr. Mariano Agusto, Dr. Franco Tassi, Dr. Thomas Darrah, Dr. Stuart Simmons, Dr. Stefano Caliro, Dr. Giovanni Chiodini, Dr. Orlando Vaselli, Dr. Alberto Caselli, Dr. Dmitri Rouwet, Dr. Johan Varekamp

Author Statement

Daniele Tardani: Conceptualization, Methodology, Validation, Investigation, Writing - original draft, Supervision. **Emilie Roulleau**: Project administration, Methodology, Validation, Investigation, Writing - review & editing. **Daniele Pinti**: Conceptualization, Methodology, Investigation, Supervision, Writing - review & editing. **Pamela Pérez-Flores**: Conceptualization, Writing - review & editing. **Linda Daniele**: Writing - review & editing. **Martin Reich**: Resources, Writing - review & editing. **Pablo Sánchez**: Writing - review & editing. **Diego Morata**: Resources, Funding acquisition, Writing - review & editing. **Luc Richard:** Methodology.